Equilibria between α- and β-Agostic Stabilized Rotamers of Secondary Alkyl Niobium Complexes

Joëlle Jaffart,[§] Michel Etienne,*[,‡] Feliu Maseras,[||] John E. McGrady,[||] and Odile Eisenstein*[,†]

Contribution from the Laboratoire de Chimie de Coordination du CNRS, UPR 8241, 205 Route de Narbonne, 31077 Toulouse Cedex 4, France, and Laboratoire de Structure et Dynamique des Systèmes Moléculaires et Solides, UMR 5636, Université de Montpellier II, 34095 Montpellier Cedex 5, France

Received October 30, 2000

Abstract: The isopropyl chloro complex $Tp^{Me2}NbCl(i\text{-}Pr)(PhC{\equiv}CMe)$ (**2**) [Tp^{Me2} = hydrotris(3,5-dimethylpyrazolyl)borate] exhibits a β-agostic structure in the crystal. The conformation of the alkyl group is such that the agostic methyl group lies in the Cα−Nb−Cl plane and the nonagostic one, in a wedge formed by two pyrazole rings. As observed by solution NMR spectroscopy, restricted rotation about the Nb−C bond allows the observation of an equilibrium between this species, **2β**, and a minor α-agostic rotamer **2α**. A putative third rotamer which would have the secondary hydrogen in the wedge is not observed. Similar behavior is observed for related $Tp'NbCl(i\text{-}Pr)(R_2C{\equiv}CMe)$ [$Tp' = Tp^{Me2}$, R_2 = Me (**3**); $Tp' = Tp^{Me2,4Cl}$, R_2 = Ph (**4**)]. The two diastereomers of the *sec*-butyl complex $Tp^{Me2}NbCl(sec\text{-}Bu)(MeC{\equiv}CMe)$ (**5**) have been separated. In the crystal, **5CR-AS** has a β-agostic methyl group with the ethyl group located in the wedge formed by two pyrazole rings. The same single β-agostic species is observed in solution. The other diastereomer, **5AR-CS** has a β-agostic methylene group in the solid state, and the methyl group sits in the wedge. In solution, an equilibrium between this β-agostic methylene complex **5AR-CSβ** and a minor α-agostic species **5AR-CSα**, where the ethyl substituent of the *sec*-Bu group is located in the wedge between two pyrazole rings, is observed. NMR techniques have provided thermodynamic parameters for these equilibria (K = **2β**/**2α** = 4.0 ± 0.1 at 193 K, $\Delta G^{o}_{193} = -2.2 \pm 0.1$, $\Delta H^{o} = -7.4 \pm 0.1$ kJ mol^{-1}, and $\Delta S^{o} = -27 \pm 1$ J K^{-1} mol^{-1}), as well as kinetic parameters for the rotation about the Nb−C bond (at 193 K, $\Delta G^{\ddagger}$(**2**) = 47.5 ± 2.5, $\Delta H^{\ddagger} = 58.8 \pm 2.5$ kJ mol^{-1}, and $\Delta S^{\ddagger} = 59.0 \pm 10$ J K^{-1} mol^{-1}). Upon selective deuteration of the β-methyl protons in $Tp^{Me2}NbCl[CH(CD_3)_2](PhC{\equiv}CMe)$ (**2**-d_6), an expected isotope effect that displaces the equilibrium toward the α-agostic rotamer is observed (K = **2**-d_6**β**/**2**-d_6**α** = 3.1 ± 0.1 at 193 K, $\Delta G^{o}_{193} = -1.8 \pm 0.1$, $\Delta H^{o} = -8.3 \pm 0.4$ kJ mol^{-1} and $\Delta S^{o} = -34 \pm 2$ J K^{-1} mol^{-1}). The anomalous values for ΔH^{o} and ΔS^{o} are discussed. Hybrid quantum mechanics/molecular mechanics calculations (IMOMM (B3LYP:MM3)) on the realistic model $Tp^{Me2}NbCl(i\text{-}Pr)(HC{\equiv}CMe)$ have reproduced the energy differences between the α- and β-agostic species with remarkable accuracy. Similar calculations show that $Tp^{Me2}NbCl(CH_2Me)(HC{\equiv}CMe)$ is α-agostic only and that $Tp^{5-Me}NbCl(CH_2Me)(HC{\equiv}CMe)$, which has no methyl groups at the 3-positions of the pyrazole rings, is β-agostic only. Analysis and discussion of the computational and experimental data indicate that the unique behavior observed for the secondary alkyl complexes stems from competition between electronic effects favoring a β-agostic structure and steric effects directing a bulky substituent in the wedge between two pyrazole rings of Tp^{Me2}. All of the secondary alkyl complexes thermally rearrange to the corresponding linear alkyl complexes via a first-order reaction.

Introduction

C−H agostic interactions[1] in transition metal alkyl complexes continue to be of high significance not only because they may model σ-alkane adducts[2] but also in their own right.[3] Importantly, they participate either in ground- or transition-state stabilization during olefin polymerization.[4] The more commonly observed β-agostic structure is adopted in the ground state of both early and late transition metal alkyl complexes. At early transition metal centers, an α-agostic interaction orientates the growing alkyl chain and lowers the barrier to its migration to the coordinated olefin.[5,6] For late transition metal catalysts however, the catalyst resting state exhibits a β-agostic interaction that is released in the transition state for alkyl migration.[7] Agostic interactions may also lie along the competing reaction coordinate, which leads to intramolecular C−H bond activation processes such as β-[8−12] or α-hydrogen elimination,[13−15]

‡ LCC Toulouse, e-mail: etienne@lcc-toulouse.fr.
† LSDSMS Montpellier, e-mail: odile.eisenstein@lsd.univ-montp2.fr.
§ CNRS.
|| Université de Montpellier.

(1) Brookhart, M.; Green, M. L. H.; Wong, L. L. *Prog. Inorg. Chem.* **1988**, *36*, 1−124.
(2) Wick, D. D.; Reynolds, K. A.; Jones, W. D. *J. Am. Chem. Soc.* **1999**, *121*, 3974−3983.
(3) Haaland, A.; Scherer, W.; Ruud, K.; McGrady, G. S.; Downs, A. J.; Swang, O. *J. Am. Chem. Soc.* **1998**, *120*, 3762−3772.
(4) Grubbs, R. H.; Coates, G. W. *Acc. Chem. Res.* **1996**, *29*, 85−93.
(5) Piers, W. E.; Bercaw, J. E. *J. Am. Chem. Soc.* **1990**, *112*, 9406−9407.
(6) Krauledat, H.; Brintzinger, H. H. *Angew. Chem., Int. Ed. Engl.* **1990**, *29*, 1412−1413.
(7) Tanner, M. J.; Brookhart, M.; DeSimone, J. M. *J. Am. Chem. Soc.* **1997**, *119*, 7617−7618.
(8) Burger, B. J.; Thompson, M. E.; Cotter, W. D.; Bercaw, J. E. *J. Am. Chem. Soc.* **1990**, *112*, 1566−1577.

10.1021/ja0038169 CCC: $20.00
Published on Web 06/01/2001

Scheme 1

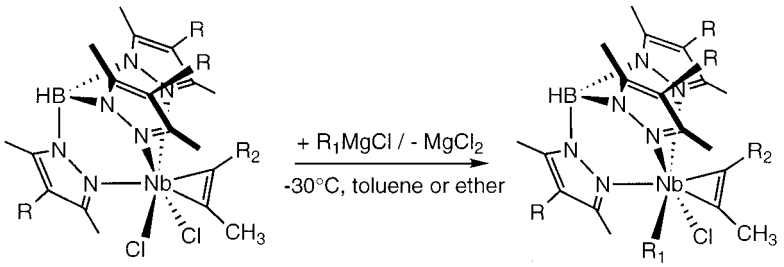

1

R_1 = *i*-Pr	R = H	R_2 = Ph	**2**
		R_2 = Me	**3**
	R = Cl	R_2 = Ph	**4**
R_1 = *sec*-Bu	R = H	R_2 = Me	**5**

several of these processes being reversible. Thus, the dichotomy between the two types of agostic interactions is a recurrent theme. Given the well-established electronic preference for a β-agostic interaction, it is not surprising that α-agostic alkyls are generally formed only in the absence of β-hydrogens. A few exceptions have, however, been found in crowded environments where the alkyl group is prevented from occupying the site necessary for a β-agostic interaction.[16,17] In addition, β-agostic interactions MCH_2CH_2-μ-H restrict rotation about the C−C bond, an in-place mechanism[18] exchanging the agostic and terminal hydrogens being inferred from detailed kinetic and thermodynamic studies. As mentioned previously, reversible β-hydrogen elimination may eventually lead to alkyl isomerization via an olefin hydride complex. β-agostic isopropyl palladium cations, models for the resting states of ethylene polymerization catalysts, have very recently been found to be more stable than the β-agostic *n*-propyl complexes with which they interconvert.[19]

Agostic interactions are, thus, at the heart of elementary processes occurring in various fundamental events in organometallic chemistry and catalysis.

The ground-state α-agostic interaction is the rule in *n*-alkyl group 5 complexes $Tp^{Me2}MCl(\mu\text{-H-}CHCH_2R)(PhC{\equiv}CR')$ (Tp^{Me2} = hydrotris(3,5-dimethylpyrazolyl)borate, M = Nb, Ta).[17,20] Interestingly, these complexes (M = Nb) undergo a reversible migratory alkyl insertion that results in an intramolecular C−C bond metathesis.[21] In all of the structures reported so far, we have observed a selective location of the alkyl substituent in a wedge formed by two pyrazolyl rings cis to the alkyl group. This relies on the unique topological properties of Tp^{Me2} which, apart from shielding the metal center thanks to a large cone angle (239°), creates three different sectors or wedges able to accommodate different substituents (wedge angle, 67°).[22] Competition between these steric and electronic effects resulted in the observation of α- and β-agostic stabilized rotamers of similar energy in an isopropyl group of $Tp^{Me2}NbCl(i\text{-Pr})(PhC{\equiv}CMe)$.[23] Herein, we provide an in-depth study of this phenomenon, including thermodynamic and kinetic data on the interconversion the rotamers. The previously reported structural data on the isopropyl complex are augmented by the successful synthesis, separation, crystal structure determination, and solution dynamics of the two diastereomers of $Tp^{Me2}NbCl(sec\text{-Bu})(MeC{\equiv}CMe)$, as well as hybrid quantum mechanics/molecular mechanics calculations on these and related systems.

Results

Synthesis of Secondary Alkyl Complexes. Secondary alkyl chloro complexes $Tp'NbCl(R_1)(R_2C{\equiv}CMe)$ [R_1 = *i*-Pr, Tp′ = Tp^{Me2}, R_2 = Ph (**2**) or Me (**3**); Tp′ = $Tp^{Me2,4Cl}$, R_2 = Ph (**4**); R_1 = *sec*-Bu, Tp′ = Tp^{Me2}, R_2 = Me (**5**)] were prepared in 55 to 80% yield via addition of the appropriate alkyl Grignard to the selected dichloro complex[24] $Tp'NbCl_2(R_2C{\equiv}CMe)$ (**1**) between −30 °C and room temperature in toluene or diethyl ether (Scheme 1). $Tp^{Me2}NbCl[CH(CD_3)_2](PhC{\equiv}CMe)$ (**2**-d_6), selectively deuterated at the methyl groups of the isopropyl ligand, was also synthesized. All Tp^{Me2} complexes are orange crystalline materials which give satisfactory elemental analysis. The $Tp^{Me2,4Cl}$ derivatives are extremely soluble, even in pentane, and are characterized only by NMR spectroscopy.

The practical aspects of the synthesis deserve comments. Following the addition of the Grignard at low temperature, the initial red-purple color characterizing the dichloro complexes slowly turned to orange. Around 0 °C, a sudden color change to violet occured, regardless of solvent. Examination of the reaction mixture by ^{1}H NMR then showed the presence of the rearranged linear alkyl complex in varying amounts (sometimes the isomerization goes to completion). The mechanism of this rearrangement is most probably a β-hydrogen elimination/reinsertion sequence. Once isolated, the secondary alkyl complexes are stable at room temperature. This indicates that the rearrangement is catalyzed in situ. We have not studied the details of this catalysis but the associated violet color suggests a redox mechanism. Adventitious unidentified zirconium species

(9) Brookhart, M.; Lincoln, D. M.; Bennett, M. A.; Pelling, S. *J. Am. Chem. Soc.* **1990**, *112*, 2691−2694.
(10) Green, M. L. H.; Sella, A.; Wong, L. L. *Organometallics* **1992**, *11*, 2650−2659.
(11) McNally, J. P.; Cooper, N. J. *Organometallics* **1988**, 7, 1704−1715.
(12) Tempel, D. J.; Brookhart, M. *Organometallics* **1998**, *17*, 2290−2296.
(13) Fellmann, J. D.; Schrock, R. R.; Traficante, D. D. *Organometallics* **1982**, *1*, 481−484.
(14) Parkin, G.; Bunel, E.; Burger, B. J.; Trimmer, M. S.; Van Asselt, A.; Bercaw, J. E. *J. Mol. Catal.* **1987**, *41*, 21−39.
(15) Schrock, R. R.; Seidel, S. W.; Mösch-Zanetti, N. C.; Shih, K.-Y.; O'Donoghue, M. B.; Davis, W. M.; Reiff, W. M. *J. Am. Chem. Soc.* **1997**, *119*, 11876−11893.
(16) Guo, Z.; Swenson, D. C.; Jordan, R. F. *Organometallics* **1994**, *13*, 1424−1432.
(17) Etienne, M. *Organometallics* **1994**, *13*, 410−412.
(18) Derome, A. E.; Green, M. L. H.; Wong, L. L. *New J. Chem.* **1989**, *13*, 747−753.
(19) Tempel, D. J.; Johnson, L. K.; Huff, R. L.; White, P. S.; Brookhart, M. *J. Am. Chem. Soc.* **2000**, *122*, 6686−6700.
(20) Hierso, J.-C.; Etienne, M. *Eur. J. Inorg. Chem.* **2000**, 839−842.
(21) Etienne, M.; Mathieu, R.; Donnadieu, B. *J. Am. Chem. Soc.* **1997**, *119*, 3218−3228.
(22) Trofimenko, S. *Scorpionates − The Coordination Chemistry of Polypyrazolylborate Ligands*; Imperial College Press: London, 1999.
(23) Jaffart, J.; Mathieu, R.; Etienne, M.; McGrady, J. E.; Eisenstein, O.; Maseras, F. *Chem. Commun.* **1998**, 2011−2012.
(24) Etienne, M.; Biasotto, F.; Mathieu, R.; Templeton, J. L. *Organometallics* **1996**, *15*, 1106−1112.

Table 1. Selected Bond Distances (Å), Angles and Torsional Angles (Deg) for **2**, **5CR-AS** and **5AR-CS**

complex	**2**	**5CR-AS**	**5AR-CS**
Nb−Cl	2.493(1)	2.4857(5)	2.4534(9)
Nb−C(l)	2.228(4)	2.223(2)	2.233(4)
Nb···C(2)	2.608(4)		2.598(2)
Nb···C(3)			2.785(5)
C(l)−C(2)	1.476(7)	1.484(3)	1.528(7)
C(1)−C(3)	1.535(6)	1.507(3)	1.470(7)
Nb···H(21)	2.17(5)	2.12(3)	
Nb−C(l)−C(2)	87.0(3)	86.6(1)	121.9(3)
Nb−C(1)−C(3)	121.2(3)	123.3(2)	95.3(3)
Cl−Nb−C(1)	122.1(1)	122.3(6)	118.7(1)
C(2)−C(1)−C(3)	115.3(4)	114.9(2)	112.7(4)
Cl−Nb−C(l)−C(2)	5.3	4.4	
Cl−Nb−C(I)−C(3)			4.3
Nb−C(l)−C(2)−H(21)	2.4	0.5	

have been proposed to catalyze a similar isomerization of zirconium alkyl complexes.[25] It is also known that CO insertion can be catalyzed by redox mechanisms[26] or assisted by Lewis acids.[27] No improvement was observed when 1,4-dioxane was added to the reaction mixture in an attempt to trap and precipitate $MgCl_2$. Despite numerous attempts to vary the reaction conditions, the only convenient way we found to prevent the rearrangement was to leave the reaction mixture in the air for ∼10 min once the orange color had been established below 0 °C. Of course, this method has the disadvantage of empiricism, and formation of linear isomers always remains a problem.

sec-Butyl complex **5** was formed in an ∼2:1 (^{1}H NMR) kinetic ratio of two diastereomers **5CR-AS** and **5AR-CS**, respectively (see X-ray crystal structures). Following the nomenclature of Sloan and co-workers, the configuration of the metal is specified first. An atomic number of 12 was assigned to the coordinated alkyne.[28,29] The use of a 2-fold excess of the Grignard allowed the preferred generation of **5CR-AS**. It was then conveniently obtained in 80% yield after crystallization from toluene/pentane mixtures. On the other hand, isolation of the minor diastereomer **5AR-CS** required careful experimental monitoring and skill. **5AR-CS** is only slightly more soluble than **5CR-AS**. Following repeated crystallizations and extractions from toluene/pentane mixtures, crystalline **5AR-CS** was isolated in 17% yield.

Crystal Structures. X-ray crystal structures for complexes **2**, **5CR-AS**, and **5AR-CS** were obtained at 160 K on an image plate diffractometer. **5CR-AS** and **5AR-CS** crystallize in the monoclinic (space group $P2_1/n$) and triclinic (space group $P\bar{1}$) systems, respectively. Selected distances and angles are gathered in Table 1. Views of the molecules are presented in Figures 1, 2 ,and 3, respectively. A distorted octahedral geometry around Nb is adopted. The (4e)-alkyne sits between two pyrazole rings in a plane roughly bisecting Cl−Nb−Cα. These features are common to the Tp′NbXY(alkyne) family.

For all three of the complexes, the most prominent feature of the structure is the presence of a β-agostic interaction. The agostic carbon (or hydrogen) is always in the Cα−Nb−Cl plane, with torsion angles in this plane never higher than 5.3°. The β-agostic interaction is characterized by an acute Nb−Cα−Cβ angle of 87.0(3)° for **2**, 86.6(1)° for **5CR-AS,** and 95.3(3)° for **5AR-CS** and Nb−Cβ distances of 2.608(4) Å for **2**, 2.598(2) Å for **5CR-AS**, and 2.789(5) Å for **5AR-CS**. In addition, the Cα−Cβ bond (∼1.48 Å) for the agostic β carbon is significantly shorter than that for the nonagostic β carbon (∼1.52 Å). This double-bond character testifies to the olefin hydride character imparted by the agostic interaction. These metric data also characterize other early[30,31] or late[32] transition metal β-agostic complexes. For compounds **2** and **5CR-AS**, the agostic hydrogen (among others) has been located from a Fourier difference map and refined isotropically. Nb−Hβ distances of 2.17(5) Å and 2.12(3) Å are observed for **2** and **5CR-AS** respectively. It must also be noted that the β-agostic interaction causes important steric constraints in the three cases. The pyrazolyl ring that splits the angle Cl−Nb−Cα is notably twisted out of the bisecting plane, with the 3-Me group displaced toward the chlorine. **2** and **5CR-AS**, both of which have a β-methyl agostic group, have very similar parameters for bonding with the metal, which suggests the nonagostic methyl and ethyl groups have a similar steric influence in the wedge. A more obtuse Nb−Cα−Cβ angle, a longer Nb−Cβ bond, a shorter Nb−Cl bond, and a smaller Cα−Nb−Cl angle observed for **5AR-CS** characterize a weaker interaction with the β-methylene agostic group.

Apart from the β-agostic structures adopted, the conformation about the niobium−α-carbon bond is to be emphasized. In complex **2**, the conformation is such that the nonagostic methyl group is located in a wedge formed by the two cis pyrazolyl rings. Similarly, in **5CR-AS**, the β-ethyl group is found in this same wedge, leaving a methyl group in the agostic position. It is worth noting that this same structural feature is also observed in the α-agostic primary alkyl complexes $Tp^{Me2}MCl(CH_2Me)$-(PhC≡CR) (M = Nb, Ta)[17,20] and $Tp^{Me2}NbCl(CH_2SiMe_3)$-(PhC≡CMe)[21] in which the alkyl group sits between two pyrazolyl rings. For **5AR-CS**, however, the situation is reversed because of the configuration change at either Nb or Cα. A β-methylene group, arising from a bulkier ethyl group, now agostically interacts with the niobium, thus providing more steric hindrance with both the metal and chlorine atoms, as indicated by the longer Nb···Cβ separation and a larger Nb−Cα−Cβ angle. In this case, the smaller, nonagostic, β-methyl group occupies the wedge. In all cases, then, the less bulky substituent, namely the secondary hydrogen, occupies the same position where it points toward the alkyne. The QM/MM calculations reported later show that these different situations arise as a result of competing steric and electronic effects.

NMR Studies. Variable temperature NMR studies on several of these secondary alkyl complexes revealed a dynamic process equilibrating two rotamers exhibiting either a β- or an α-agostic interaction. Importantly, this process is highly dependent on the respective configuration at Nb and Cα in the case of the diastereomers of **5**. We start with a structural discussion before moving to the dynamics itself. The isopropyl complex **2** will serve as a lead and is described first.

Because of restricted rotation about the Nb−alkyne bond, the NMR spectra of all of the phenylpropyne complexes appear as two sets of signals of unequal intensity at all temperatures ($\Delta G_{rot} > 68$ kJ mol^{-1}).[24] For the sake of clarity, we will discuss only the major alkyne rotamer, which is depicted in the schemes,

(25) Chirik, P. J.; Day, M. W.; Labinger, J. A.; Bercaw, J. E. *J. Am. Chem. Soc.* **1999**, *121*, 10308−10317.
(26) Magnuson, R. H.; Meirowitz, R.; Zulu, S. J.; Giering, W. P. *J. Am. Chem. Soc.* **1982**, *104*, 5790.
(27) Richmond, T. G.; Basolo, F.; Schriver, D. F. *Inorg. Chem.* **1982**, *21*, 1272.
(28) Brown, M. F.; Cook, B. R.; Sloan, T. E. *Inorg. Chem.* **1975**, *14*, 1273.
(29) Zelewsky, A. V. *Stereochemistry of Coordination Compounds*; Wiley: Chichester, 1996.
(30) Dawoodi, Z.; Green, M. L. H.; Mtetwa, V. S. B.; Prout, K.; Schultz, A. J.; Williams, J. M.; Koetzle, T. F. *J. Chem. Soc., Dalton Trans.* **1986**, 1629−1637.
(31) Jordan, R. F.; Bradley, P. K.; Baenziger, N. C.; LaPointe, R. E. *J. Am. Chem. Soc.* **1990**, *112*, 1289−1291.
(32) Carr, N.; Mole, L.; Orpen, A. G.; Spencer, J. L. *J. Chem. Soc., Dalton Trans.* **1992**, 2653−2662.

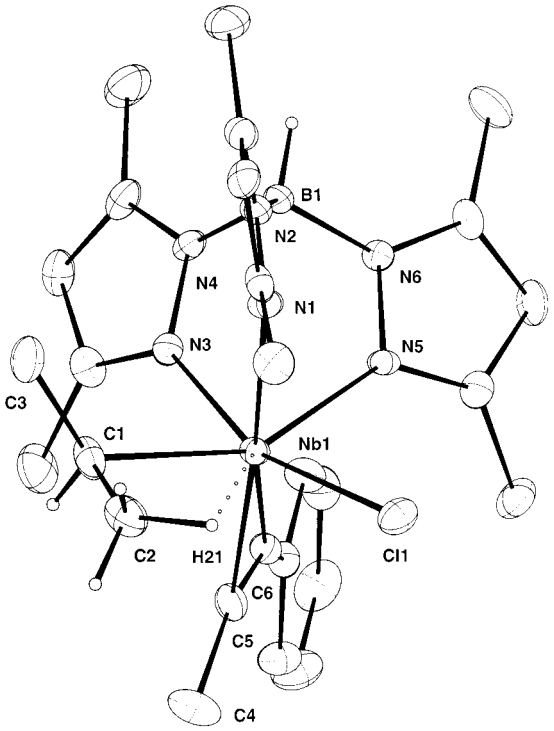

Figure 1. Plot of the molecular structure of $Tp^{Me2}NbCl(i\text{-}Pr)(Ph\text{-}C{\equiv}CMe)$ (**2**). Located and refined hydrogens are shown.

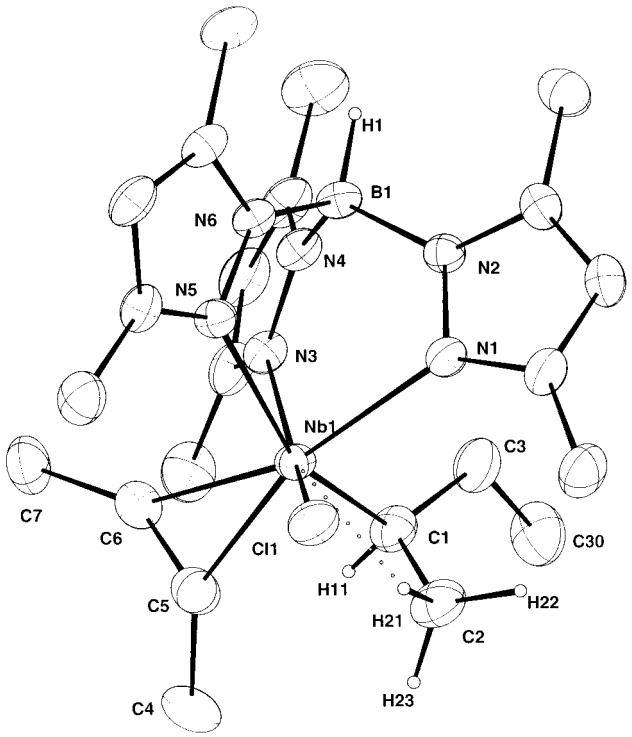

Figure 2. Plot of the molecular structure of $Tp^{Me2}NbCl(sec\text{-}Bu)(Ph\text{-}C{\equiv}CMe)$ (**5CR-AS**). Located and refined hydrogens are shown.

but all of the conclusions are valid for the minor one. Cooling down a dichloromethane-d_2 solution of **2** led to broadening and eventually to a coalescence and sharpening of all of the ^{1}H NMR signals into two sets of unequal intensity (Figure 4). The alkyne methyl signal appearing at δ 3.48 at 303 K split into two below 233 K. In the slow exchange limit (193 K), these alkyne signals were observed at δ 3.08 and 3.62 (4:1 ratio, respectively). The most abundant species, **2*β***, exhibited a β-agostic interaction, as observed in the solid state, whereas the minor one, **2α**, was

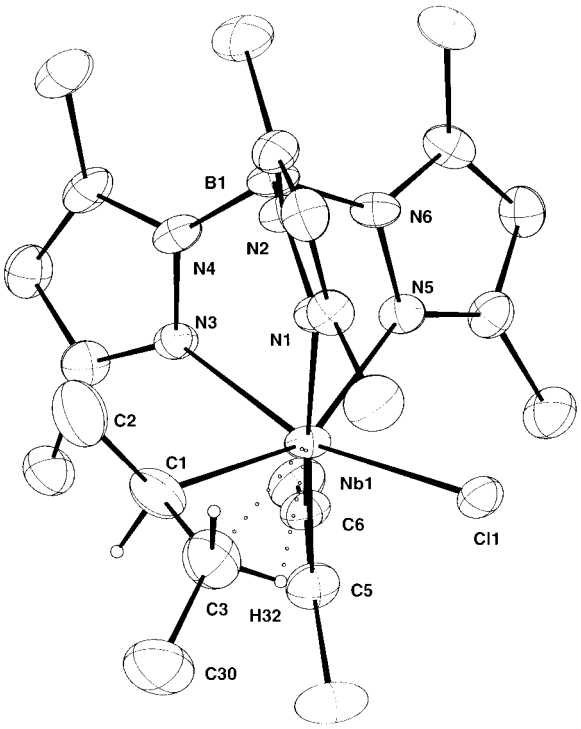

Figure 3. Plot of the molecular structure of $Tp^{Me2}NbCl(sec\text{-}Bu)(Ph\text{-}C{\equiv}CMe)$ (**5AR-CS**). Located and refined hydrogens are shown, except H(32).

α-agostic (Scheme 2). The methine and methyl signals of the isopropyl group of **2*β*** were observed at δ 2.10 (multiplet) and δ 1.29 and 0.06 (both doublets, $^2J_{HH}$ = 7 Hz), respectively. These Cβ methyl signals correlated (^{1}H−^{13}C HMQC) to ^{13}C NMR signals at δ 6.0 and 20.7 (d, $^1J_{CH}$ = 123 Hz), respectively. The Cα methine ^{13}C NMR signal appeared as a doublet ($^1J_{CH}$ = 141 Hz) at δ 72.0. This rehybridization at Cα constitutes the strongest evidence for the β-agostic interaction in solution, because as observed in several early transition metal β-agostic complexes, the in-place rotation of the β-agostic methyl group is not frozen out. Note that the agostic methyl has the most shielded ^{13}C NMR signal but the most deshielded ^{1}H NMR signal. This assignment is also in accord with the *sec*-butyl analysis below. For the d^0 β-agostic ethyl complex $[(\eta^5\text{-}C_5H_4\text{-}Me)_2Zr(CH_2CH_2\text{-}\mu\text{-}H)(PMe_3)]^+$, Cα resonates at δ 28.6 ($^1J_{CH}$ = 141 Hz), and Cβ appears at δ −6.9 ($^1J_{CH}$ = 123 Hz).[33] Rotamer **2α** is characterized by a shielded ^{1}H NMR multiplet (δ −1.13). In the ^{13}C NMR spectrum, a somewhat Nb-broadened Cα signal appears as a deshielded doublet (δ 126.4) with a reduced $^1J_{CH}$ of 100 ± 5 Hz. Related α-agostic alkyl compounds, such as $Tp^{Me2}MCl(\mu\text{-H-CHR})$(alkyne) (M = Nb, Ta)[20,21] and $Ta(\mu\text{-H-CHCMe}_3)(C_2H_4)(PMe_3)_2$ have similar NMR parameters.[13] It must be emphasized here that, as depicted in Scheme 2, a putative third rotamer with the α hydrogen in the wedge and a methyl group in the Cα−Nb−Cl plane (which could or could not have a β-agostic stucture) is not detected by ^{1}H NMR. Similar data and conclusions are valid for complexes **3** and **4** containing 2-butyne in place of phenylpropyne or $Tp^{Me2,4-Cl}$ in place of Tp^{Me2}, respectively.

Table 2 provides thermodynamic data obtained after conventional treatment of experimental NMR data acquired at different temperatures (see Supporting Information). Equilibrium constants were measured from the integration of alkyne methyl signals. It is seen that **2*β*** is favored on enthalpic grounds (ΔH^o

(33) Alelyunas, Y. W.; Guo, Z.: LaPointe, R. E.; Jordan, R. F. *Organometallics* **1993**, *12*, 544−553.

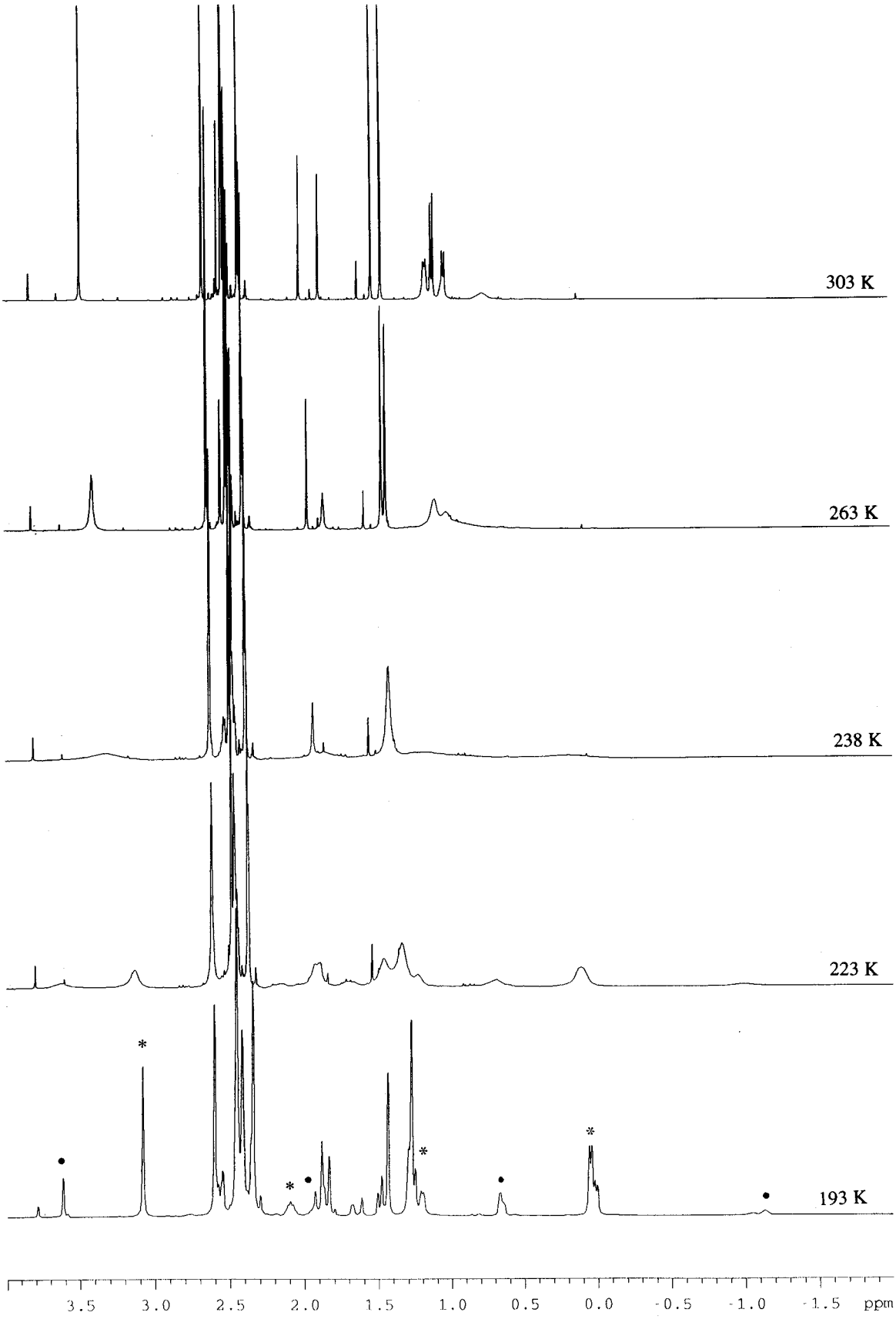

Figure 4. Expanded region of the variable temperature ^{1}H NMR spectrum of $Tp^{Me2}NbCl(i\text{-}Pr)(PhC{\equiv}CMe)$ (**2**) (400 MHz, dichloromethane-d_2). Alkyne methyl, isopropyl methyl and methine signals for the major alkyne rotamer are highlighted: asterisk (*), β-agostic rotamer; solid dot, (•) α-agostic rotamer.

$= -7.4 \pm 0.1$ kJ mol^{-1}), whereas entropy favors **2α** ($\Delta S^o = -27 \pm 1$ J K^{-1} mol^{-1}). β-Agostic stabilized rotamers are more favored in the 2-butyne complex **3** or the $Tp^{Me2,4-Cl}$ complex **4**. A thermodynamic isotope effect is observed, as seen from

Scheme 2

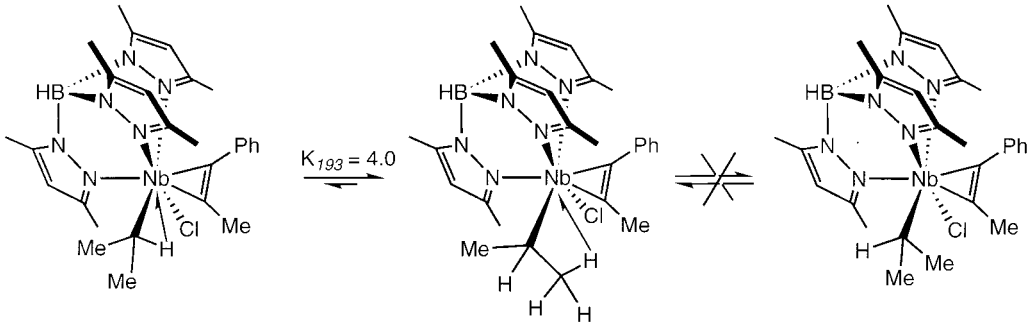

2α **2**β

Table 2. Thermodynamic Parameters for the Equilibria between *o*- and *p*-Agostic Rotamers

compd	*K*	ΔG^o (kJ mol^{-1})	ΔH^o (kJ mol^{-1})	ΔS^o (J K^{-1} mol^{-1})
2[a]	4.0 ± 0.1	−2.2 ± 0.1	−7.4 ± 0.1	−27 ± 1
2-d_6[a]	3.1 ± 0.1	−1.8 ± 0.1	−8.3 ± 0.4	−34 ± 2
3[b]	14 ± 2	−4.0 ± 0.3		
4[a]	14 ± 2	−4.2 ± 0.2	−9.7 ± 0.9	−28 ± 5
5AR-CS[a]	2.5 ± 0.2	−1.5 ± 0.3	−3.7 ± 0.3	−11 ± 2

[a] *K* and ΔG^o at 193 K [b] *K* and ΔG^o at 183 K.

the data for **2** and **2**-d_6. On the basis of the lower zero point energy of the C−D bond, we might anticipate a slight preference for the lighter H atom to occupy the agostic position, a phenomenon that has been observed in other species.[1,44] The observed ratio of $K_{H_{193}}/K_{D_{193}} > 1$ is, therefore, entirely expected, because deuteration of the methyl groups should cause a shift toward the α-agostic isomer. However, a closer examination of the thermodynamic parameters indicates that it is solely entropic reasons that force $K_{H_{193}}$ to be greater than $K_{D_{193}}$, and in fact, ΔH^o is more negative in **2**-d_6 than it is in **2**. Thus, we reach the counterintuitive conclusion that, on enthalpic grounds alone, D should prefer to be involved in the agostic position at the expense of H. Although we have no definitive explanation for this observation, we will return to this point in the later discussion.

Even more interestingly, the two diastereomers **5CR-AS** and **5AR-CS** do not behave similarly. **5CR-AS** is *β*-agostic in solution, as in the solid state (Scheme 3). In the ^{1}H NMR spectrum, there is only a slight line broadening and sharpening upon cooling, with no splitting of the signals. In the low-temperature (193 K) ^{1}H NMR spectrum, the *β*-agostic methyl group gives a doublet ($^1J_{HH}$ = 7 Hz) at *δ* 1.16, which correlates with a ^{13}C NMR signal at *δ* 4.1. The in-place rotation is not stopped, so that the $^1J_{CH}$ of 123 Hz does not prove the agostic interaction. Cα resonates as a doublet at *δ* 79.4 in the ^{13}C NMR spectrum. The $^1J_{CH}$ of 144 Hz then testifies to the *β*-agostic interaction. The nonagostic diastereotopic methylene protons appear as a shielded multiplet centered at *δ* −0.26. HMQC ^{1}H−^{13}C allows the assignment of the nonagostic methylene and methyl groups at *δ* 28.5 and 18.3, respectively. Significantly, this experiment showed that there is no other rotamer present here. There is, thus, a very high barrier to rotation about the Nb−C bond, as depicted in Scheme 3.

For **5AR-CS**, an equilibrium between two rotamers, **5AR-CSα** and **5AR-CS*β***, exhibiting either an α- or a *β*-agostic interaction, respectively, is observed (Scheme 4). Evidence is provided below that in **5AR-CS*β***, the methylene group, not the methyl group, is *β*-agostic in solution as well as in the crystal (see above). A temperature-dependent ^{1}H NMR spectrum reveals a dynamic process akin to that observed for **3** (or **2**, but with only one type of alkyne rotamer). Again, the alkyne methyl signals are good qualitative and quantitative probes. At room temperature, they are observed at *δ* 3.15 and 1.92. They broaden and then split below 218 K. In the slow exchange limit, they give signals at *δ* 2.93 and 1.73 for the *β*-agostic rotamer **5AR-CS*β*** and at *δ* 3.19 and 1.89 for the α-agostic species **5AR-CSα**. The equilibrium constant K_{193} is 2.5 (ΔG^o_{193} = −1.5 kJ mol^{-1}). It is less shifted toward the *β*-agostic form than it is in the case of the isopropyl complex **3** (K_{183} = 14, Table 2). This emphasizes the increased steric pressure in the Cl−Nb−Cα plane, where the agostic interaction, which now involves the methylene group, takes place. It is remarkable that again, only two rotamers are present. The third potentially viable rotamer, which would have the secondary hydrogen in the wedge formed by the two cis pyrazolyl rings, is not observed (Scheme 4).

In the ^{1}H NMR spectrum (193 K) of **5AR-CS*β***, two broadened signals having partially resolved fine structure at *δ* 1.47 and 0.86 characterize the diastereotopic methylene protons. In the ^{13}C NMR spectrum, Cβ appears as a triplet centered at *δ* 14.4 with an averaged $^1J_{CH}$ = 123 Hz. Cα resonates at *δ* 82.1 as a doublet. For Cα, the magnitude of $^1J_{CH}$ = 132 Hz, smaller than those for the *β*-agostic isopropyl complexes, suggests a weaker interaction. The nonagostic *β*-methyl group gives a ^{1}H NMR doublet at *δ* 0.05 ($^2J_{HH}$ = 7 Hz) and a ^{13}C NMR quartet *δ* 19.0. These values compare well with those for the nonagostic methyl group of the isopropyl complexes. **5AR-CSα** is unequivoqually characterized by a shielded ^{1}H NMR signal for Hα at *δ* −1.14 and a deshielded ^{13}C NMR signal for Cα appearing at *δ* 126.4 with a low $^1J_{CH}$ (92 Hz).

Spin saturation transfer expriments (SST)[34−36] at different temperatures were used to obtain kinetic parameters for the process interconverting the rotamers. Reliable data were obtained for the isopropyl complex **2** and the *sec*-butyl complex **5AR-**

(34) Forsen, S.; Hoffman, R. A. *J. Chem. Phys.* **1963**, *39*, 2892.
(35) Mann, B. E. *J. Magn. Res.* **1976**, *21*, 17−23.
(36) Brookhart, M.; Lamanna, W.; Humphrey, M. B. *J. Am. Chem. Soc.* **1982**, *104*, 2117−2126.
(37) Maseras, F.; Morokuma, K. *J. Comput. Chem.* **1995**, *16*, 1170−1179.
(38) Ujaque, G.; Cooper, A. C.; Maseras, F.; Eisenstein, O.; Caulton, K. G. *J. Am. Chem. Soc.* **1998**, *120*, 361−365.
(39) Maseras, F. *Top. Organomet. Chem.* **1999**, *4*, 165−191.
(40) Maseras, F. *Chem. Commun.* **2000**, 1821−1827.
(41) Han, Y.; Deng, L.; Ziegler, T. *J. Am. Chem. Soc.* **1997**, *119*, 5939−5945.
(42) Weiss, H.; Ehrig, M.; Ahlrichs, R. *J. Am. Chem. Soc.* **1994**, *116*, 4919−4928.
(43) Lohrenz, J. C. W.; Woo, T. K.; Ziegler, T. *J. Am. Chem. Soc.* **1995**, *117*, 12793−12800.
(44) Calvert, R. B.; Shapley, J. R. *J. Am. Chem. Soc.* **1978**, *100*, 7726−7727.

Scheme 3

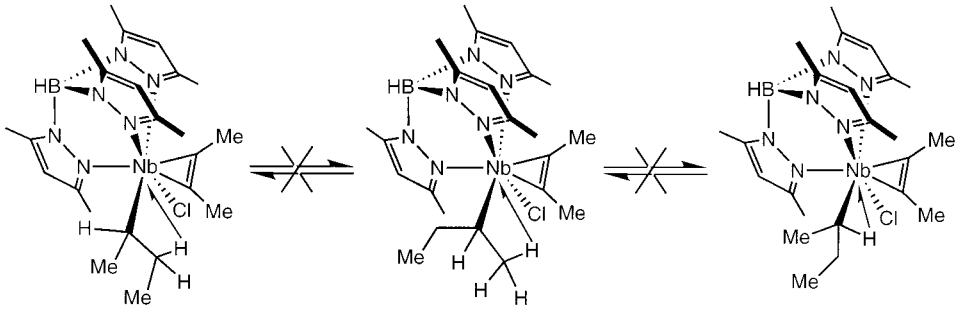

5*CR-AS*

Scheme 4

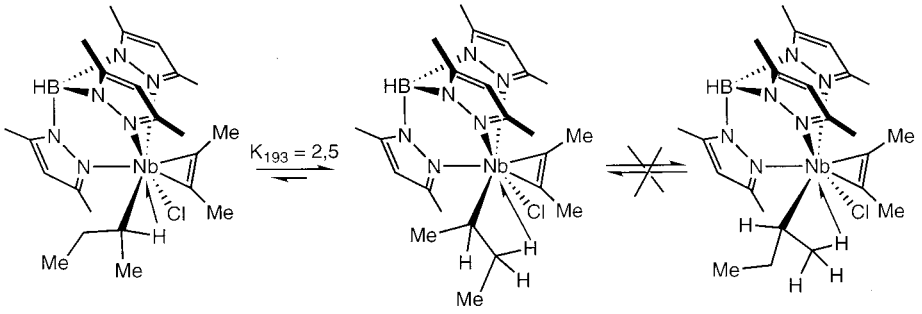

5*AR-CS*α **5*AR-CS*β**

CS. Note that the alkyne rotation is so slow at these temperatures that it may be neglected. Saturation of the deshielded alkyne methyl group of the β-agostic rotamer (for example, at δ 3.08 for **2**β or δ 2.93 for **5AR-CS*β*** at 193 K) and observation of the intensity decrease of the alkyne methyl signal for the α-agostic rotamer provides a determination of $k_{\beta\rightarrow\alpha}$. Attempts at measuring $k_{\alpha\rightarrow\beta}$ by saturation of the α-agostic signal did not give satisfactory data, presumably because of intramolecular NOE interactions.

Activation parameters were obtained through conventional treatment of the experimental data (see Supporting Information). High barriers to rotation around the Nb−Cα bond were observed (for **2**, $E_a = 60.0 \pm 2.5$ kJ mol^{-1}, $\Delta H^{\ddagger} = 58.8 \pm 2.5$ kJ mol^{-1}, and $\Delta G^{\ddagger}$(193 K) $= 47.5 \pm 2.5$ kJ mol^{-1}; for **5AR-CS**, $E_a = 60.0 \pm 2.5$ kJ mol^{-1}, $\Delta H^{\ddagger} = 56.0 \pm 2.5$ kJ mol^{-1}, and $\Delta G^{\ddagger}$(193 K) $= 41 \pm 2$ kJ mol^{-1}). The barriers for the conversion β-→α-agostic rotamers are similar for both isopropyl and *sec*-butyl ligands, although they are slightly lower for **5AR-CS**. Quite high positive entropies of activation of 59 ± 10 and 75 ± 10 J K^{-1} mol^{-1} are observed for **2** and **5AR-CS**, respectively, which points to a less ordered transition state in which the agostic interaction is lost (i.e., a dissociative process).

Reactivity. We previously showed that α-agostic *n*-alkyl complexes Tp′NbCl(CH_2R)(PhC≡CMe) thermally rearrange to methyl complexes Tp′NbCl(Me)(PhC≡CCH_2R) via a rate-determining reversible migratory insertion of the alkyl group onto the alkyne.[21] In contrast, compounds arising from the migratory insertion onto the alkyne are not observed (^{1}H NMR) for the secondary alkyl compounds that are the subject of this paper, but instead, isomerization of the secondary alkyl group to a primary one occurs. For example, when isopropyl complexes **2**−**4** are heated in toluene at 323 K, the known α-agostic *n*-alkyl complexes Tp′NbCl(CH_2CH_2Me)(R_2C≡CMe) are formed according to Scheme 5. Similarly, a mixture of the *sec*-butyl compounds **5CR-AS** and **5AR-CS** rearrange to the α-agostic

Scheme 5

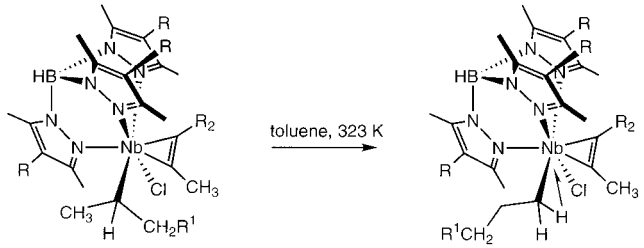

R_1 = H	R = H	R_2 = Ph	**2**	**6**
		R_2 = Me	**3**	**7**
	R = Cl	R_2 = Ph	**4**	**8**
R_1 = CH_3	R = H	R_2 = Me	**5**	**9**

n-butyl Tp^{Me2}NbCl($CH_2CH_2CH_2$Me)(MeC≡CMe) (**9**). The new compounds **7**−**9** are identified by comparison with authentic samples prepared via addition of either *n*-propyl MgCl or *n*-butyl MgCl to the appropriate Tp′$NbCl_2$(alkyne) complex. They all exhibit features characteristic of α-agostic structures (see Experimental Section).[21]

The rearrangement of **2** was followed by ^{1}H NMR in toluene-d_8 at 323 K. The disappearance of **2** is first-order with $k_{H_{323}} = (2.7 \pm 0.2) \times 10^{-5}$ s^{-1} ($\Delta G^{\ddagger} \approx 108$ kJ mol^{-1}). Several unidentified decomposition products are observed, together with the *n*-propyl complex and some propene. Consequently, the kinetics are well-behaved for about two half-lives only, and attempts at monitoring the decomposition at higher temperatures met with no success. A kinetic isotope effect of 1.6 was obtained from the decomposition of **2**-d_6 [$k_{D_{323}} = (1.7 \pm 0.2) \times 10^{-5}$ s^{-1}]. The mechanism of the reaction is, thus, most probably a rate-determining β hydrogen elimination reaction that first gives a transient α-olefin hydride intermediate, which then undergoes fast reinsertion of the olefin, yielding a more stable *n*-alkyl derivative. Because the availability of pure **5CR-AS** is very limited, we were not able to compare the rate of its rearrange-

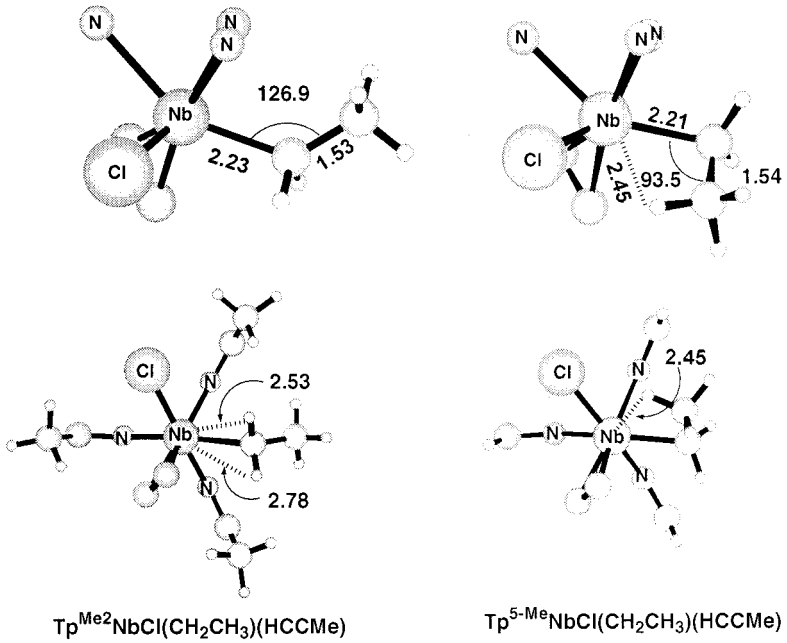

Figure 5. IMOMM-computed structures of $Tp^{Me2}Cl(CH_2CH_3)(HC{\equiv}CMe)$ and $Tp^{5-Me}NbCl(CH_2CH_3)(HC{\equiv}CMe)$ with distances in Å and angles in degrees. In each case, views from the side and along the trigonal axis are shown. In the side view, all atoms other than the alkyl group and those attached directly to the Nb center have been ommitted for clarity. For the view down the trigonal axis, the methyl groups in the 5 position of the pyrazole ring are also included to illustrate the steric crowding of the agostic site.

Scheme 6

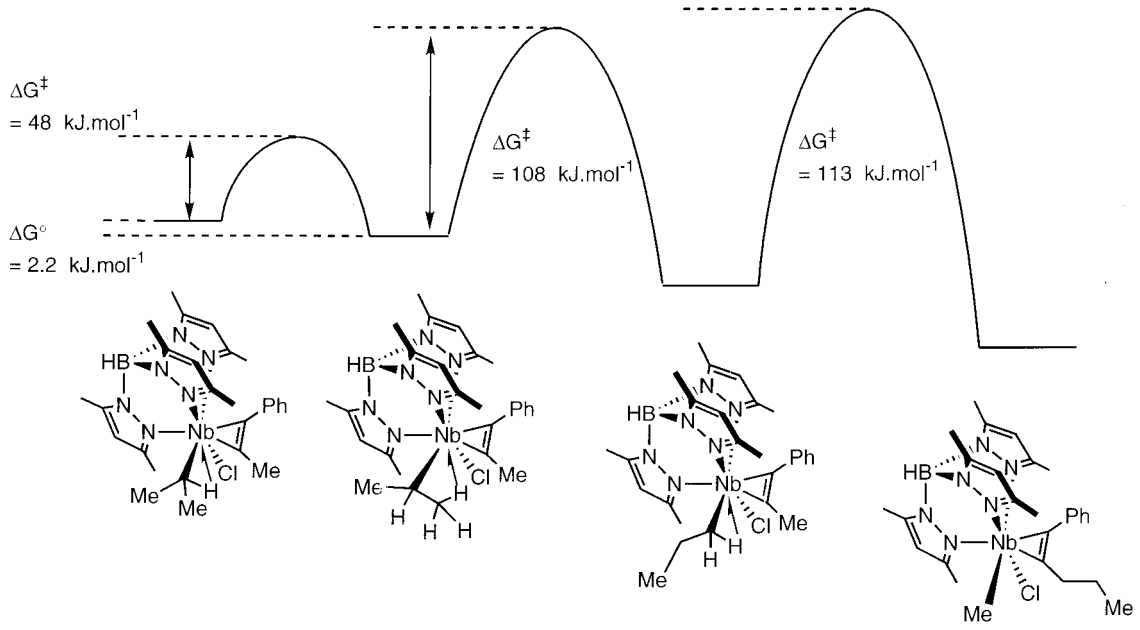

ment with that of its diastereomer, **5AR-CS.** In summary, secondary alkyl niobium complexes exhibiting α- and *β*-agostic structures of similar energy do not undergo migratory insertion of the alkyl group. They rearrange via *β*-hydrogen elimination to their more stable α-agostic linear isomers, which then can exchange alkyl groups. The whole chemistry we observe is summarized in Scheme 6, with the rightmost event taken from previous work.[21]

Theoretical Calculations. Integrated quantum mechanics/molecular mechanics (IMOMM)[37] calculations, which have proved successful for the theoretical study of transition metal systems,[38−40] were carried out in order to try to understand the presence of only α-agostic *primary* alkyls on one hand and, on the other hand, the occurrence of both α- and *β*-agostic stabilized rotamers in *secondary* alkyls. They show how competition between electronic effects, which favor *β*-agostic structures, and steric effects, which favor a large substituent in the wedge formed by two pyrazolyl rings, is at the heart of the observed experimental behavior. The crucial role played by the 3-methyl groups in Tp^{Me2} is also highlighted.

The optimized structure of $Tp^{Me2}NbCl(CH_2CH_3)(HC{\equiv}CMe)$ is shown in Figure 5. The geometry about the α carbon is highly distorted, with a Nb−Cα−C*β* angle of 126.9° (cf. 129.8° experimentally)[17] and a small Nb−Cα−Hα1 angle (92.6°). These angular deformations, along with a slight elongation of the Cα−Hα1 bond (1.11 Å), result in a short Nb···Hα1 distance of 2.53 Å, which is consistent with the presence of a significant α-agostic interaction. The agostic hydrogen atom (Hα1) is directed toward the chloride ligand, but its nonagostic counterpart, Hα2 (Nb···Hα2 = 2.78 Å) points toward the coordinated

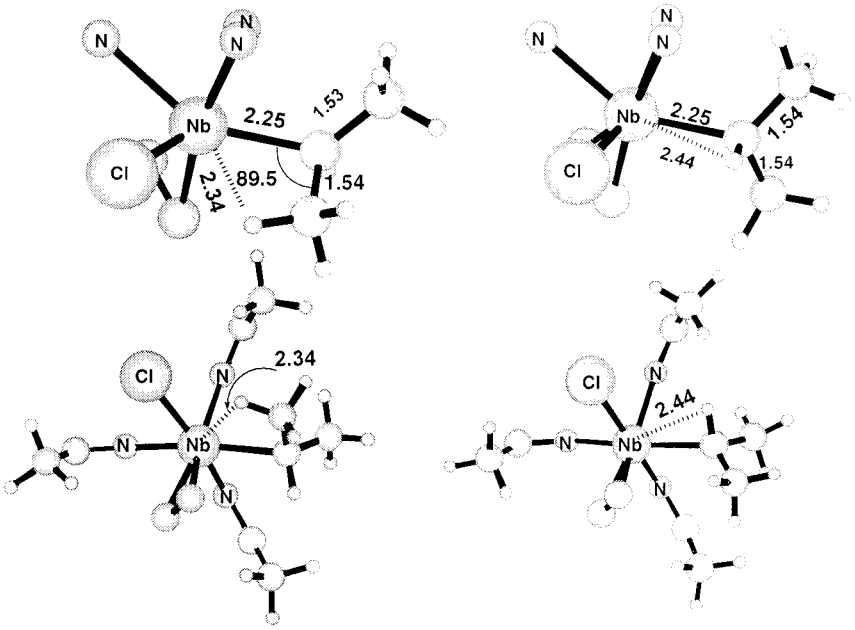

Figure 6. IMOMM-computed structure for the β- and α-agostic rotamers of $Tp^{Me2}NbCl[CH(CH_3)_2](HC{\equiv}CMe)$ with distances in Å and angles in degrees. The views shown are identical to those in Figure 5.

alkyne. The preference for this orientation can be rationalized in terms of the relative energies of the three dπ orbitals of the approximately octahedral complex. Of these three orbitals, the one that lies orthogonal to the Nb−Cl axis avoids the destabilizing π-donor influence of the chloride ligand and is also stabilized by back-bonding to the alkyne. This orbital is, therefore, the most stable of the three and is occupied by the two d electrons of Nb^{III}. The two remaining orbitals are vacant and, in principle, available to accommodate the agostic interaction; however, one of these lies in the plane orthogonal to the Nb−Cα bond, and is, therefore, inefficiently oriented for overlap with the C−H bond. The one remaining dπ orbital lies in the Cα−Nb−Cl plane, which causes the agostic interaction to be directed approximately along the bisector of the Cα−Nb−Cl angle. The opening of this angle from the perfect octahedral value of 90.0° to 111.7° is consistent with a rehydridization of the metal orbitals to allow optimal overlap of donor and acceptor orbitals.

The preference for the α-agostic structure over its β-agostic counterpart can be traced to the steric constraints imposed by the Tp^{Me2} ligand. The pendant methyl groups located at the 3 positions of Tp^{Me2} divide the opposite face of the octahedron into three approximately equivalent wedges, along one of which the Nb−Cα bond lies. Steric repulsions between Tp^{Me2} and the alkyl chain are minimized when the largest substituent on the α carbon (CH_3 in this case) is aligned along the wedge and, therefore, away from the pendant methyl groups. This steric locking of the ethyl group forces one of the α hydrogens to lie approximately along the bisector of the Cl−Nb−Cα bond, giving the experimentally observed α-agostic structure. A rotation of ∼120° about the Nb−Cα bond, giving a β-agostic structure, would place the alkyl chain in closer proximity to Tp^{Me2}, thereby increasing unfavorable steric interactions with the pendant methyl groups. Thus, the observed α-agostic structure reflects the fact that the steric factors (favoring α) dominate the electronic preference for a β-agostic structure. This hypothesis was further tested by optimizing the structure of the closely related system, $Tp^{S-Me}NbCl(CH_2CH_3)(HC{\equiv}CMe)$ [Tp^{5-Me} = hydridotris(5-methylpyrazolyl)borate]. Thus, Tp^{5-Me} differs from Tp^{Me2} only in the absence of the methyl groups in the 3 position. In this case, only a β-agostic rotamer is located on the potential energy surface (Figure 5), characterized by a Nb···Hβ separation of 2.45 Å, which is 0.08 Å shorter than that in the corresponding α-agostic structure. The β-agostic architecture also brings the agostic hydrogen in much closer contact with the chloro ligand (2.70 Å vs 3.36 Å), which results in substantial nonbonded interactions. As a result, the Cl−Nb−Cα angle is even larger than in the α-agostic structure (122.3° vs 111.7°), and the Nb−Cl bond length increases by 0.06 Å. Although the structural changes observed in interconverting the α- and β-agostic isomers are relatively subtle, in a delicately balanced situation such as this, they may have profound influence on the position of equilibrium.

It is important to note here that, despite the success in modeling the structure of the α-agostic group, the geometry of the remainder of the niobium coordination sphere is less well reproduced. The Nb−Cl bond length is underestimated by 0.128 Å, and all three Nb−N bonds are overestimated by a similar margin. Polarization functions were added to the chlorine center to attempt to rectify this problem, but that resulted in only slight improvements. Nevertheless, trends within the series of Nb−N bonds are well-reproduced, with the longest lying trans to the alkyne. Moreover, similar errors in Nb−Cl and Nb−N bond lengths emerge for all of the species described in this work, and so it is likely that the systematic shift in these bond lengths do not invalidate our conclusions relating to the agostic equilibrium.

Two distinct minimums were located on the potential energy surface of $Tp^{Me2}NbCl[CH(CH_3)_2](HC{\equiv}CMe)$, one corresponding to the crystallographically characterized β-agostic isomer **2*β*** and the other to an α-agostic isomer (Figure 6), which has been characterized spectroscopically as **2α**. The structure of the α-agostic isomer is very similar to that reported above for the ethyl analogue (Figure 5). The additional methyl group on the alkyl chain lies to one side of the alkyl chain, and in order to

Scheme 7

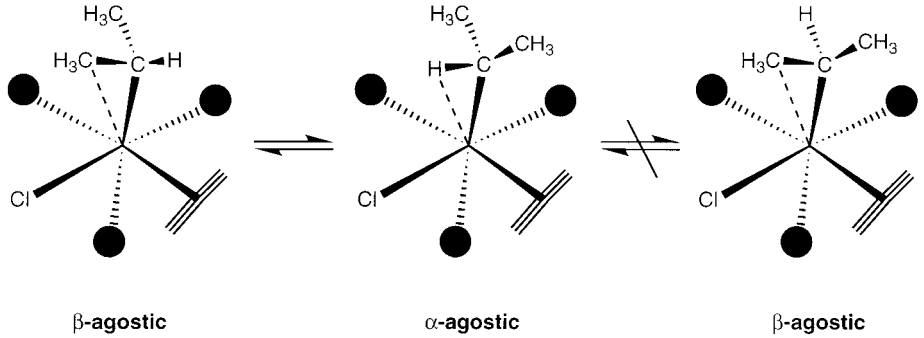

minimize steric repulsions with the Tp^{Me2} ligand, the Nb−Cα−Cβ angle opens out to 119.1°. This, in turn, causes the Nb−Cα−Hα1 angle to become more acute, reducing the Nb···H distance to 2.44 Å (cf. 2.53 Å in the ethyl analogue). The comparison of the β-agostic isopropyl structure (Figure 6) with its ethyl analogue (Figure 5) is less straightforward, because in the latter, the pendant methyl groups of the Tp^{Me2} ligand are absent. Nevertheless, it is clear that the structures are again remarkably similar, which is consistent with the fact that the additional nonagostic methyl substituent on the α carbon lies in the least sterically demanding site, along the wedge, and consequently, has minimal influence on the remainder of the molecule. The β-agostic isomer is calculated to be more stable than its α-agostic counterpart by 9.3 kJ mol^{-1}, in accord with the experimentally observed excess of the β-agostic isomer. Comparison with the experimental ΔH^o of −7.4 kJ mol^{-1} (for **2**) to −9.7 kJ mol^{-1} (for **4**) is excellent. The relative stability of the two rotamers depends on both the inherent stability of the α- and β-agostic bonds and also the steric constraints enforced by the pendant methyl groups. The close nonbonded C···C contacts between the alkyl group and the Tp^{Me2} ligand summarized in Scheme 7 suggest that the β-agostic isomer is the more sterically hindered of the two. The methyl group lies only 3.45 Å away from one of the pendant methyl groups, and the opening of the Cl−Nb−Cα angle to accommodate the agostic methyl group moves the α carbon toward the opposite methyl group, resulting in a C···C separation of only 3.38 Å. In contrast, the shortest nonbonded C···C distances in the α-agostic system are over 3.6 Å. In summary, steric factors favor the α-agostic isomer, thus resulting in its presence in equilibrium with the electronically more stable β-agostic structure.

Discussion

The observation of two energetically close α- and β-agostic stabilized rotamers of a given alkyl group is unique. Given the significance of both types of interactions in fundamental organometallic processes, it is important to delineate the factors that influence this equilibrium. First of all, both experimental and computational results substantiate the fact that β-agostic interactions are electronically preferred, whereas α-agostic interactions are sterically driven. Going one step further, we note that there is no evidence, either experimental or theoretical, for the third rotamer shown in Scheme 2, which also corresponds to a β-agostic structure in the case of the isopropyl complex. This conformation would place the smallest substituent on the α carbon (i.e., H) in the least sterically hindered position, along the wedge, while forcing the two methyl groups to occupy the crowded positions to either side of the alkyl chain.

The case of the two diastereomers of **5** is highly revealing. **5CR-AS** shows a single β-methyl agostic rotamer, whereas for **5AR-CS**, both α-CH and β-methylene agostic isomers are observed. The three putative rotamers of each of the two diastereomers are summarized in Schemes 3 and 4. For **5CR-AS** (Scheme 3), the most stable conformation has the ethyl group along the wedge, and the smaller methyl and hydrogen substituents occupy the more hindered positions on either side of the alkyl chain. The α-agostic isomer, which is observed in the isopropyl analogue, is destabilized by the strong steric interactions that would result from placing the bulky ethyl substituent in the proximity of the pendant Tp^{Me2} methyl groups. The third rotamer can be discounted, because it places the hydrogen group in the least hindered position. In summary, in **5CR-AS**, placing the largest substituent (ethyl) along the wedge results in the favored β-agostic interaction. The observed structure is, therefore, favored on both electronic and steric grounds, and so only one rotamer is observed. The situation is more complex in **5AR-CS** (Scheme 4) because steric locking of the ethyl group along the wedge forces a less electronically favorable α-agostic interaction. The more favorable β-agostic interaction can only be achieved at the expense of placing the ethyl group in a less sterically favorable position. In **5AR-CS**, therefore, steric and electronic factors are opposed, and as a result, two rotamers are observed. Such marked differences have never been noted in seemingly simple organometallic systems. Clearly, they govern the interactions between alkyl groups and transition metals prior to any bond forming or bond cleavage processes and, thus, insert nicely into dynamic schemes of transition metal−alkyl complexes.

A closer inspection of the thermodynamic parameters (Table 2) of the equilibria confirms that β-agostic rotamers are preferred on enthalpic grounds. For a given alkyne (phenylpropyne), the more electron-withdrawing $Tp^{Me2,4Cl}$ in **3**, as compared with Tp^{Me2} in **2**, shifts the equilibrium further toward the β-agostic rotamer and ΔH^0 increases by 2 kJ mol^{-1}. Complex **4**, which has 2-butyne instead of phenylpropyne, also shows a larger preference for the β-agostic rotamer. The reason for this behavior is not apparent; however, for a given alkyne and Tp′ set, placing an ethyl group (agostic methylene) instead of a methyl group in the β-agostic position has a dramatic influence. The β-agostic interaction becomes much weaker in **5AR-CS** than it is in **4**, as was discussed on the basis of the structural parameters, and accordingly, ΔH^o is higher for **4** (−9.7 kJ mol^{-1}) than it is for **5AR-CS** (−3.7 kJ mol^{-1}). The difference between the two equilibria also has some of its origin in entropy factors that favor α-agostic isomers because they are less vibrationally constrained arrangements in α-agostic structures. When going from **4** to **5AR-CS**, the smaller difference in ΔS^o accompanies the decrease in $\Delta H°$.

Although our work reports the first and unique experimental observation of both α- and β-agostic rotamers of a single alkyl

group, there have been attempts to quantify their relative stabilities in other systems. β-agostic isomers have been computed (relativistic DFT level) to be more stable than α-agostic ones in group 9 d^6 ethyl complexes $CpM(PH_3)(CH_2CH_2)(CH_2CH_3)^+$ by 55 (M = Co), 34 (M = Rh) and 18.4 (M = Ir) kJ mol^{-1}.[41] A similar trend for d^0 early transition metal has resulted from calculations for $Cp_2Ti(CH_2CH_2CH_3)^+$ in a study of ethylene insertion into the Ti−CH_3 bond of $Cp_2TiCH_3^+$. At the MP2 level, the α-agostic *n*-propyl isomer was found to be less stable than the β-agostic one by 56 kJ mol^{-1}.[42] In a parallel investigation at the DFT level, the α-agostic *n*-butyl isomer of $Cp_2Zr(CH_2CH_2CH_2CH_3)^+$ was found to be 46.8 kJ mol^{-1} higher than the β-agostic isomer. Interestingly, the energy difference shrinks to a maximum of 4.9 kJ mol^{-1} in ethylene adducts $CpZr(CH_2CH_2)(CH_2CH_3)^+$,[43] and the α-agostic complex is just 9 kJ mol^{-1} below the transition state for C−C bond formation.

We observe a normal thermodynamic (or equilibrium) isotope effect (EIE) (at 193 K, $K_H/K_D = 1.29$ for the formation of the β-agostic species) favoring the formation of **2α** over **2*β*** upon deuteration of the β-position, as far as equilibrium constant K or Gibbs free energy, ΔG^o, are concerned. This trend is expected on the basis of zero-point energy (i.e., ΔH^o) differences, as a result of which the heavier deuterium prefers the stronger terminal bond, as compared to the lighter hydrogen.[1,44] However consideration of ΔH^o and ΔS^o values yields the somewhat surprising result that the EIE is "normal" only for entropic reasons ($\Delta S^o_H - \Delta S^o_D = 7 \pm 3$ J K^{-1} mol^{-1}), whereas counter-intuitively, it is "inverse" ($\Delta H^o_H - \Delta H^o_D = 0.9 \pm 0.5$ kJ mol^{-1}) on enthalpic grounds. It should be noted here that the common analysis concentrates on the C−H(D) bond, thereby neglecting the M−H(D) conterpart. The whole M−H + C−H bonding has to be taken into account, and it is, indeed, stronger in the coordinated (agostic) mode. The thermodynamic, zero-point energy preference for the inherently stronger bonding deuterium atom to occupy the more strongly bound position will preferentially place this in the agostic site. An inverse EIE ($K_H/K_D = 0.59$) for the relief of the β-agostic interaction, that is, normal ($K_H/K_D = 1.69$) for the formation of the β-agostic interaction, has been observed in the related $[(C_5Me_5)Co(CH_2CH_2\text{-}\mu\text{-}H)P(OMe)_3]^+$ system.[7] The equilibrium favoring an agostic ethyl group as opposed to a terminal structure, is shifted toward the terminal structure upon full deuteration of the ethyl protons. However, the temperature dependence of this EIE has not been studied. Relief of agostic interaction leads to similar inverse EIE in other systems, although the nonagostic species is not observed.[45,46] A survey of the recent literature in this field reveals that the interpretation of EIEs in organometallic systems is by no means straigthforward. Inverse EIEs (i.e., $K_H/K_D < 1$) have been taken as evidence for alkane σ-complex formation prior to alkane loss in reductive elimination of alkane from alkyl hydride complexes.[2,47] Inverse EIEs have been observed for alkane coordination prior to oxidative addition to give the alkyl hydride complexes,[48,49] with one recent exception.[50] Counter-intuitively, inverse EIEs have also been observed for the binding of dihydrogen[51,52] or ethylene[53] to transition metal centers. The in-depth interpretation of these effects points to the crucial role played by vibrational modes other than simply stretching modes, and rotational motions involving either H or D at both enthalpic and entropic levels.[53,54] As described in the results section, the interpretation of the EIE for **2** has been reduced to the comparison between one free or terminal C−H(D) bond (in **2α**) and one agostic (in **2*β***) C−H(D) bond, and this simplification might be too crude. For example the rehybridization of the alkyl group from sp^3 to sp^2 that accompanies the β-agostic interaction is not taken into account. Thus, other isotope-sensitive modes add to the higher-energy C−H(D)-stretching vibration, and their contribution might be important in the case of this secondary EIE. The fact that D is smaller than H might also play a role in these congested molecules. Thus, we are reluctant to propose a definitive explanation for the apparent discrepancies between thermodynamic parameters of the EIE for **2**. Clearly, more work is needed to develop a full understanding of isotope effects for agostic compounds.

Barriers to rotation about metal−carbon bonds are usually considered as low. A recent study of the fluxional behavior of η^3-allyl derivatives of highly crowded meso *ansa*-scandocenes indicates that the barrier to the rotation about the Sc−C bond of an η^1-allyl intermediate is much smaller than the smallest η^3/η^1 interconversion barrier of ∼45 kJ mol^{-1}.[55] When such restricted rotations have been observed, barriers have not been systematically measured. This is somewhat surprising, because as stated in the Introduction, this is an essential event that is needed to properly describe the dynamics of alkyl groups that are bound to transition metal centers. High barriers to rotation about the Nb−C bonds, of the order of 60 kJ mol^{-1}, are observed for the secondary alkyl complexes reported herein. Enthalpies of activation are similar for both **2** and **5AR-CS**. The quite high entropy of activation for such a process obtained in both cases points to a transition state in which the agostic interaction is released. The difference between $\Delta S^‡$ values for **2** and for **5AR-CS** is certainly not significant within experimental errors. These dissociative processes thus allow an upper limit for the strength of these agostic interactions to be assessed by the measure of $\Delta H^‡$ (∼60 kJ mol^{-1}). A 40 kJ mol^{-1} barrier to rotation about the Pd−C bond in the β-agostic isopropyl complex $\{(ArN{=}C(R)\text{-}C(R){=}NAr)Pd[CH(CH_2\text{-}\mu\text{-}H)CH_3]\}^+$ has been reported.[12] This barrier is of the same order of magnitude as that for the in-place rotation exchanging the agostic hydrogens. Other transition-state parameters were not reported. In the proposed unsaturated intermediate $Cp_2Nb(CHMe_2)$, which allows scrambling of hydrogens in $Cp_2NbH(C_2H_3CH_3)$, an upper estimate of the barrier to rotation of 24 kJ mol^{-1} has been obtained.[10] A "high" barrier to Re−C or W−C bond rotation in the presumed β-agostic intermediates $\{CpRe(CO)_2[CH_3CH(CH_2\text{-}\mu\text{-}H)]\}^+$/$Cp_2W[CH_3CH(CH_2\text{-}\mu\text{-}H)]\}^+$ has been inferred from the failure to observe "fast" deuterium/proton incorporation in the methyl groups of $CpRe(CO)_2(CH_3CH{=}CH_2)$[56]/$Cp_2W(CD_3CD{=}CD_2)$,[11] respectively, upon protonation by CF_3CO_2H/D. However, none of these experimental data allow a clear assessment of the relative importance of the steric effects and

(45) Fryzuk, M. D.; Haddad, T. S.; Rettig, S. J. *Organometallics* **1991**, *10*, 2026−2036.
(46) Cook, K. S.; Piers, W. E.; Rettig, S. J.; McDonald, R. *Organometallics* **2000**, *19*, 2243−2245.
(47) Hall, C.; Perutz, R. N. *Chem. Rev.* **1996**, *96*, 6, 3125−3146.
(48) Schultz, R. H.; Bengali, A. A.; Tauber, M. J.; Weiller, B. H.; Wasserman, E. P.; Kyle, K. R.; Moore, C. B.; Bergman, R. G. *J. Am. Chem. Soc.* **1994**, *16*, 7369−7377.
(49) Bengali, A. A.; Schultz, R. H.; Moore, C. B.; Bergman, R. G. *J. Am. Chem. Soc.* **1994**, *116*, 9585−9589.
(50) Geftakis, S.; Ball, G. E. *J. Am. Chem. Soc.* **1998**, *120*, 9953−9954.
(51) Hascall, T.; Rabinovitch, D.; Murphy, V. J.; Beachy, M. D.; Friesner, R. A.; Parkin, G. *J. Am. Chem. Soc.* **1999**, *121*, 11402−11417.
(52) Bender, B. R.; Kubas, G. J.; Jones, L. H.; Swanson, B. I.; Eckert, J.; Capps, K. B.; Hoff, C. D. *J. Am. Chem. Soc.* **1997**, *119*, 9179−9190.
(53) Bender, B. R. *J. Am. Chem. Soc.* **1995**, *117*, 11239−11246.
(54) Abu-Hasanayn, F.; Krogh-Jespersen, K.; Goldman, A. S. *J. Am. Chem. Soc.* **1993**, *115*, 8019−8023.
(55) Abrams, M. B.; Yoder, J. C.; Loeber, C.; Day, M. W.; Bercaw, J. E. *Organometallics* **1999**, *18*, 1389−1401.
(56) Casey, C. P.; Yi, C. S. *Organometallics* **1991**, *10*, 33−35.

the strength of the agostic interactions in the barrier to rotation of the alkyl groups.

Finally, we find that, although stable at room temperature, secondary alkyl niobium complexes rearrange to linear α-agostic alkyl ones via a rate-determining reversible *β*-hydrogen elimination ($k_{323} = 2.7\ 10^{-5}\ s^{-1}$, $k_H/k_D = 1.6$). This can be compared with the rate of the *β*-hydrogen elimination in $Cp^*_2Sc(CH_2CH_2Me)$ ($k_{265} = 7.9\ 10^{-5}\ s^{-1}$) and a kinetic isotope effect of 2.0 for $Cp^*_2Sc(CH_2CH_2Ph)$.[8] Recently observed secondary alkyl zirconocene complexes, such as $Cp_2ZrCl[CH(CH_3)CH_2Me]$, also rearrange to linear alkyl complexes $Cp_2ZrCl(CH_2CH_2CH_2Me)$ over the course of several hours at 296 K.[25] $(C_5H_3SiMe_2)_2ZrCl[CH(CH_3)_2]$ isomerizes to $(C_5H_3SiMe_2)_2ZrCl[CH_2CH_2CH_3]$ above 283 K.[57] These rearrangements of secondary alkyls follow a general trend ascribed to steric relief. Interestingly, *β*-agostic isopropyl cationic palladium complexes $\{(diimine)Pd[CH(CH_3)_2]\}^+$ have recently been found to be more stable (∼5 kJ mol^{-1}) than their linear *β*-agostic isomers $[(diimine)Pd(CH_2CH_2CH_3)]^+$.[19] This trend was reversed upon addition of an olefin, the agostic interaction then being lost. An upper limit for the barrier to the isomerization was determined to be 44 kJ mol^{-1}.

Summary. The results we describe herein can be summarized by the energy diagram shown in Scheme 6. It is the first time that α- and *β*-agostic isomers of similar energy have been observed. The main reason for this behavior stems from the topology of Tp′ ligands. Hybrid QM/MM calculations and experimental data have produced a detailed description of the system at both qualitative and quantitative levels. Our results are particularly significant given the central role played by the dynamics of alkyl groups in organometallic chemistry and catalysis. Finally, we call for further work aimed at probing equilibrium isotope effects in related agostic systems.

Experimental Section

All experiments were carried out under a dry dinitrogen atmosphere using either Schlenck tube or glovebox techniques. THF and diethyl ether were obtained after refluxing purple solutions of Na/benzophenone under dinitrogen. Toluene, *n*-hexane, pentane, 1,4-dioxane and dichloromethane were dried by refluxing over CaH_2 under dinitrogen. Deuterated NMR solvents were dried over molecular sieves, degassed by freeze-pump-thaw cycles and stored under dinitrogen. Data are reported in dichloromethane-d_2 unless otherwise stated. ^1H and ^{13}C NMR spectra were obtained on Bruker AM 250, DPX 300, and AMX 400 spectrometers. Only pertinent $^1J_{CH}$ are quoted in the ^{13}C spectra. Because of the sometimes extreme complexity of the spectra, several signals might not be observed. Elemental analyses were performed in the analytical service of our Laboratory. $Tp^{Me2}NbCl_2(PhC{\equiv}CMe)$, $Tp^{Me2}NbCl_2(MeC{\equiv}CMe)$ and $Tp^{Me2,4Cl}NbCl_2(PhC{\equiv}CMe)$ were prepared according to published procedures.[24,58] Grignard reagents (RMgCl in diethyl ether) were either purchased or synthesized via classical procedures. $CH(CD_3)_2Cl$ was synthesized from acetone-d_6 and then converted to $[CH(CD_3)_2]MgCl$ in diethyl ether according to published procedures.[11,59]

$Tp^{Me2}NbCl(CHMe_2)(PhC{\equiv}CMe)$ (2). The same procedure was used to prepare all of the secondary alkyl complexes. A solution of $(CHMe_2)MgCl$ in diethyl ether (2.5 mL, 0.6 M, 1.5 mmol) was added dropwise via syringe to a cooled (−30 °C, ethanol/liquid nitrogen bath) diethyl ether solution (50 mL) of $Tp^{Me2}NbCl_2(PhC{\equiv}CMe)$ (0.580 g, 1.0 mmol). The color of the solution gradually changed from purple-red to orange as the temperature slowly rose to 0 °C. Stirring was maintained at this temperature for ∼1 h. Air was then admitted into the flask for ∼10 min by removing the septum under static vacuum. Dioxane (1 mL) then hexane (10 mL) were added, and the solution was degassed several times. A white precipitate formed immediately. The slurry was filtered through a pad of Celite to give a clear orange solution, which was evaporated to dryness. The residue was dissolved in a minimum amount of toluene (∼2 mL). Addition of hexane (∼6 mL) yielded orange crystals (0 °C, overnight) which were collected by filtration, washed with small amounts of pentane, and dried under vacuum (0.430 g, 0.74 mmol, 74%). Anal. Calcd for $C_{27}H_{37}N_6ClBNb$: C, 55.45; H, 6.38; N, 14.37. Found: C, 55.63; H, 6.53; N, 14.23. IR (KBr): ν(C−H) 2960−2860 cm^{-1} (m, Tp^{Me2} and $NbCHMe_2$). ^1H NMR (400 MHz): at 303 K, major rotamer *δ* 7.2 (m, 3H, *Ph*C≡CMe), 6.89 (d, 2H, *Ph*C≡CMe), 5.97, 5.82, 5.63 (s, 1H each, Tp^{Me2}*CH*), 3.48 (s, 3H, PhC≡C*Me*), 2.66, 2.53, 2.52, 2.42, 1.52, 1.46 (s, 3H each, Tp^{Me2}*Me*), 1.15 (d, $^3J_{HH} = 6$ Hz, 3H, CH*Me*$_2$), 1.10 (d, $^3J_{HH} = 7$ Hz, 3H, CH*Me*$_2$), 0.76 (br, 1H, C*H*Me$_2$); minor rotamer *δ* 7.93 (d, 2H, *o*-*Ph*C≡CMe), 7.56 (t, 2H, *m*-*Ph*C≡CMe), 7.40 (t, 1H, *p*-*Ph*C≡CMe), 5.98, 5.95, 5.80 (s, 1H each, Tp^{Me2}C*H*), 2.66, 2.57, 2.51, 2.41, 2.01, 1.88 (s, 3, 3, 6, 3, 3H, Tp^{Me2}*Me* and PhC≡C*Me*), 1.05 (br, part. overlap, 3H, CH*Me*$_2$), 1.02 (d, $^3J_{HH} = 6.5$ Hz, 3H, CH*Me*$_2$); rotamer ratio, 2.0; at 193 K, because of overlaps, some signals were obscured or unassignable; major rotamer for **2*β***, *δ* 5.92, 5.80, 5.65 (s, 1H each, Tp^{Me2}C*H*), 3.08 (s, 3H, PhC≡C*Me*), 2.61, 2.46, 2.42, 2.35, 1.44, 1.28 (s, 3H each, Tp^{Me2}*Me*), 2.10 (m, 1H, C*H*Me$_2$), 1.29 (part. overlap, 3H, CH*Me*$_2$), 0.06 (d, $^3J_{HH} = 7$ Hz, 3H, CH*Me*$_2$); for **2α**, *δ* 5.97, 5.81, 5.59 (s, 1H each, Tp^{Me2}C*H*), 3.62 (s, 3H, PhC≡C*Me*), 2.55, 2.37, 2.30, 1.49, 1.30 (s, 3H each, Tp^{Me2}*Me*), 1.88 (obscured, 3H, CH*Me*$_2$), 0.68 (d, $^3J_{HH} = 4.5$ Hz, 3H, CH*Me*$_2$), −1.13 (m, 1H, C*H*Me$_2$); **2*β***/**2α** = 4.00; minor rotamer for **2*β***, *δ* 5.98, 5.90, 5.85 (s, 1H each, Tp^{Me2}C*H*), 2.46, 2.41, 1.89, 1.84, 1.26 (s, 3H each, Tp^{Me2}*Me* and PhC≡C*Me*), 1.93 (m br, 1H, C*H*Me$_2$), 1.21 (d, $^2J_{HH} = 7$ Hz, 3H, CH*Me*$_2$), 0.02 (d, $^3J_{HH} = 7$, 3H, CH*Me*$_2$); for **2α**, *δ* 5.95, 5.75 (s, 1H each, Tp^{Me2}C*H*), 2.58, 2.56, 1.93, 1.87, 1.62 (s, 3H each, Tp^{Me2}*Me* and PhC≡C*Me*), 1.68 (d, $^3J_{HH} = 4.5$ Hz, 3H, CH*Me*$_2$), 0.65 (d, $^3J_{HH} = 4.5$ Hz, 3H, CH*Me*$_2$), −1.05 (m br, 1H, C*H*Me$_2$); **2*β***/**2α** = 3.60; rotamer ratio, 2.0. ^{13}C NMR (100 MHz, 1.93K): major rotamer for **2*β***, *δ* 221.8, 203.9 (Ph*C*≡*C*Me), 151.7, 151.1, 148.3, 145.1, 143.6, 143.5 (Tp^{Me2}C*Me*), 107.6, 107.1, 106.2 (Tp^{Me2}*CH*), 72.0 (d, $^1J_{CH} = 142$ Hz, NbC*H*Me$_2$), 20.7 (q, $^1J_{CH} = 123$ Hz, NbCH*Me*$_2$), 19.6 (≡C*Me*), 15.6, 15.0, 13.9, 13.1, 13.05, 13.0 (Tp^{Me2}*Me*), 6.0 (q, $^1J_{CH} = 123$ Hz, NbCH*Me*$_2$); HMQC correlates protons at *δ* 1.29 and 0.06 with carbons at *δ* 6.0 and 20.7, respectively; for **2α**, *δ* 244.2, 213.7 (Ph*C*≡*C*Me), 151.2, 150.9, 144.4, 143.8 (Tp^{Me2}C*Me*), 126.4 (br d, $^1J_{CH} = 100 \pm 5$ Hz, NbC*H*Me$_2$), 107.4, 107.2 (Tp^{Me2}*CH*), 33.1, 28.1 (q each, $^1J_{CH} = 123$ Hz, NbCH*Me*$_2$), 24.0 (≡C*Me*); HMQC correlates proton at *δ* −1.13 with carbon at *δ* 126.4; minor rotamer for **2*β***, *δ* 213.7, 210.1 (Ph*C*≡*C*Me), 151.0, 150.7, 148.0, 145.1, 144.8, 143.9 (Tp^{Me2}C*Me*), 107.5, 106.3 (Tp^{Me2}*CH*), 71.5 (d, $^1J_{CH} = 138$ Hz, NbC*H*Me$_2$); for 2α, signals hardly assignable; the following are for **2*β*** (major rotamer) and **2α** (minor rotamer): 15.5, 14.7, 14.6, 14.5, 14.3, 14.1, 13.5, 13.3, 12.7.

$Tp^{Me2}NbCl[CH(CD_3)_2](PhC{\equiv}CMe)$ (2-d_6). IR (KBr): ν(C−H) 2960−2900 (m, Tp^{Me2} and $NbCH(CD_3)_2$), ν(C−D) 2250−2120 (w, $NbCH(CD_3)_2$), 2059 (m, $NbCH(CD_3)_2$) cm^{-1}. ^1H NMR (400 MHz): Tp^{Me2} and alkyne signals not significantly different from those for **2**; at 293 K, major rotaimerm *δ* 0.65 (br, 1H, *CH*$(CD_3)_2$); rotamer ratio, 2.0; at 193 K, major rotamer for **2*β***-d_6, *δ* 2.07 (br d, 1H, *CH*$(CD_3)_2$); for **2α**-d_6, −1.17 (br d, 1H, C*H*$(CD_3)_2$); **2*β***-d_6/**2α**-d_6 = 3.08; minor rotamer for **2*β***-d_6, *δ* 1.93 (br m, 1H, C*H*$(CD_3)_2$); for **2α**-d_6, −1.08 (br, 1H, C*H*$(CD_3)_2$); rotamer ratio, 2. ^{13}C NMR (100 MHz, 193K): major rotamer for **2*β***-d_6, *δ* 71.8 (d, $^1J_{CH} = 142$ Hz, Nb*C*H$(CD_3)_2$), 19.5 (br, $w_{1/2} = 80$ Hz, NbCH(*C*$D_3)_2$), 5 (br, $w_{1/2} = 80$ Hz, NbCH(*C*$D_3)_2$); for **2α**-d_6, *δ* 126.0 (d, $^1J_{CH} = 97 \pm 5$ Hz, Nb*C*H$(CD_3)_2$), 32.3 (br, $w_{1/2} = 80$ Hz, NbCH(*C*$D_3)_2$), 5 (br, $w_{1/2} = 80$ Hz, NbCH(*C*$D_3)_2$); minor rotamer for **2*β***-d_6, *δ* 71.3 (d, $^1J_{CH} = 142$ Hz, Nb*C*H$(CD_3)_2$); unobserved for **2α**-d_6.

$Tp^{Me2}NbCl(CHMe_2)(MeC{\equiv}CMe)$ (3). Anal. Calcd for $C_{22}H_{35}N_6ClBNb$: C, 50.55; H, 6.70; N, 16.08. Found: C, 50.28; H, 6.45; N, 16.07. IR (KBr): ν(C−H) 2960−2736 cm^{-1} (m, Tp^{Me2} and $NbCHMe_2$). ^1H NMR (400 MHz): at 293 K, *δ* 5.91, 5.90, 5.77 (s, 1H each, Tp^{Me2}C*H*), 3.00, 1.85 (s, 3H each, *Me*C≡C*Me*), 2.58, 2.47, 2.36, 2.30, 1.88 (s, 3, 6, 3, 3, 3H each, Tp^{Me2}*Me*), 1.91 (br, part. obscured, 1H,

(57) Fernandez, F. J.; Gomez-Sal, P.; Manzanero, A.; Royo, P.; Jacobsen, H.; Berke, H. *Organonmetallics* **1997**, *16*, 1553.
(58) Jaffart, J.; Nayral, C.; Choukroun, R.; Mathieu, R.; Etienne, M. *Eur. J. Inorg. Chem.* **1998**, 425−428.
(59) Condon, F. E. *J. Am. Chem. Soc.* **1951**, *73*, 4675.

C*H*Me$_2$), 1.04 (br d, 3H, CH*Me*$_2$), 0.87 (br d, 3H, CH*Me*$_2$); at 183 K, for **3*β***, *δ* 5.87, 5.84, 5.82 (s, 1H each, Tp^{Me2}*CH*), 2.68 (s, 3H, ≡C*Me*), 2.50, 2.37, 2.35, 2.29, 2.23, 1.90 (s, 3H each, Tp^{Me2}*Me*), 1.93 (part. obscured, 1H, C*H*Me$_2$), 1.59 (s, 3H, ≡C*Me*), 1.10 (d part. obscured, 3H, CH*Me*$_2$), −0.05 (d, $^3J_{HH}$ = 7 Hz, 3H, CH*Me*$_2$); for **3α**, *δ* 5.91, 5.89, 5.70 (s, 1H each, Tp^{Me2}*CH*), 3.16 (s, 3H, ≡C*Me*), 2.43, 2.39, 2.24, 2.17, 1.87, 1.81, 1.78 (s, 3H each, ≡C*Me* and Tp^{Me2}*Me*), 1.75 (d, $^3J_{HH}$ = 4.3 Hz, 3H, CH*Me*$_2$), 0.57 (d, $^2J_{HH}$ = 4.3 Hz, 3H, CH*Me*$_2$), −1.37 (m, 1H, C*H*Me$_2$); **3*β*/3α** = 16. ^{13}C NMR (100 MHz, 193 K): for **3*β***, *δ* 218.5, 211.9 (Me*C*≡*C*Me), 151.0, 150.9, 147.8, 145.0, 143.8, 143.6 (Tp^{Me2}C*Me*), 107.4, 107.0, 106.2 (Tp^{Me2}*CH*), 70.55 (d, $^1J_{CH}$ = 141 Hz, Nb*C*HMe$_2$), 20.2 (q, $^1J_{CH}$ = 120 Hz, NbCH*Me*$_2$), 20.4, 18.05, 15.6, 15.5, 13.7, 13.05, 13.0, 12.90 (Tp^{Me2}*Me* and *Me*C≡C*Me*), 5.61 (q, $^1J_{CH}$ = 120 Hz, NbCH*Me*$_2$); HMQC correlates protons at *δ* 1.10 and −0.05 with carbons at *δ* 20.21 and 5.61, respectively; for **3α**, signals hardly assignable as a result of overlaps and low intensity; HMQC correlates proton at *δ* −1.37 with carbon at *δ* 123.5 (d, $^1J_{CH}$ = 96 ± 10 Hz, Nb*C*HMe$_2$).

Tp^{Me2Cl}NbCl(CHMe$_2$)(PhC≡CMe) (4). ^{1}H NMR (400 MHz, 203 K): major rotamer for **4*β***, *δ* 7.15−7.29 (m. 5 H, *Ph*C≡CMe), 3.16 (s, 3H, PhC≡C*Me*), 2.68, 2.48, 2.40, 2.35, 1.51, 1.39 (s, 3H each, Tp^{Me2}*Me*), 2.13 (m, 1H, C*H*Me$_2$), 1.33, 0.11 (br d, 3H, CH*Me*$_2$); for **4α**, 0.75 (m, 3H, CH*Me*$_2$), −1.05 (m, 1H, C*H*Me$_2$); **4*β*/4α** = 16.00; minor rotamer for **4*β***, *δ* 7.80 (d, 2H, *m-Ph*C≡CMe), 7.55 (t, 2H, *o-Ph*C≡CMe), 7.39 (t, 1H, *p-Ph*C≡CMe), 2.54, 2.47, 2.38, 2.35, 1.95 (s, 3H each, Tp^{Me2}*Me*), 1.91 (PhC≡C*Me*), 1.29 (br d, 3H, C*H*Me$_2$); rotamer ratio, 2.1. ^{13}C NMR (100 MHz, 193K): major rotamer for **4*β***, *δ* 222.8, 203.7 (Ph*C*≡*C*Me), 148.9, 148.1, 145.6, 141.9, 140.3, 143.5 (Tp^{Me2}C*Me*), 137.6 (*C*ipsoPh), 128.6, 127.8, 124.9 (Tp^{Me2}*C*Cl), 110.2, 109.7, 109.0 (Tp^{Me2}*C*Cl), 72.7 (d, $^1J_{CH}$ = 140 Hz, Nb*C*HMe$_2$), 21.1 (q, $^1J_{CH}$ = 123 Hz, NbCH*Me*$_2$), 19.9 (≡C*Me*), 20.8, 13.9, 13.7, 12.3, 11.1, 11.0 (Tp^{Me2}*Me*), 5.6 (q, $^1J_{CH}$ = 123 Hz, NbCH*Me*$_2$); HMQC correlates protons at *δ* 1.33 and 0.11 with carbons at *δ* 5.6 and 21.1, respectively; for **4α**, the only assignable signal at *δ* 129.9 correlates (HMQC) with the proton signal at *δ* −1.05; minor rotamer *δ* 213.8, 209.9 (Ph*C*≡*C*Me), 148.0, 147.7, 145.0, 140.6, 140.2, 137.3 (Tp^{Me2}C*Me*), 110.1, 109.8, 109.1 (Tp^{Me2}*C*Cl), 72.1 (d, $^1J_{CH}$ = 140 Hz, Nb*C*HMe$_2$), 20.7, 20.6, 14.1, 13.8, 12.9, 11.0, 10.8 (q each, $^1J_{CH}$ = 123 Hz, NbCH*Me*$_2$) 6.31 (q, $^1J_{CH}$ = 123 Hz, NbCH*Me*$_2$).

Tp^{Me2}NbCl[CH(Me)(CH$_2$Me)](MeC≡CMe) (5CR-AS and 5AR-CS). Following the general procedure, a 2:1 mixture of **5CR-AS** and **5AR-CS** was obtained in the form of orange crystals. Anal. Calcd for $C_{23}H_{37}N_6BClNb$: C, 51.47; H, 6.95; N, 15.67. Found: C, 51.41; H, 6.69; N, 15.54. For **5CR-AS**: following the general procedure described above, reaction between Tp^{Me2}NbCl$_2$(MeC≡CMe) (0.250 g, 0.485 mmol) and *sec*-BuMgCl (1.0 mL of a 2 M solution, 2.0 mmol) yielded a 10:1 mixture of **5CR-AS** and **5AR-CS**, respectively, as ascertained by ^{1}H NMR of the crude reaction mixture. Recrystallization from toluene/pentane afforded orange crystals of **5CR-AS** (0.190 g, 0.35 mmol, 72%). ^{1}H NMR (300 MHz): at 293 K, *δ* 5.93, 5.90, 5.81 (s, 1H each, Tp^{Me2}*CH*), 2.92, 1.96 (s, 3H each, *Me*C≡C*Me*), 2.60, 2.49, 2.48, 2.38, 2.33, 1.82 (s, 3H each, Tp^{Me2}*Me*), 1.21 (d, $^3J_{HH}$ = 7 Hz, 3H, CH*Me*), 0.60 (br d, 3H, CH$_2$*Me*), 0.30 (br d, 1H, C*H*Me), C*H*$_2$Me not observed; at 193 K, *δ* 5.92, 5.86, 5.84 (s, 1H each, Tp^{Me2}C*H*), 2.73, 1.94 (s, 3H each, C*Me*), 2.53, 2.42, 2.40, 2.33, 2.27, 1.65 (s, 3H each, Tp^{Me2}*Me*), 1.86 (m, 1H, C*H*Me), 1.16 (d, $^3J_{HH}$ = 7 Hz, 3H, CH*Me*), 0.46 (t, $^3J_{HH}$ = 7 Hz, 3H, CH$_2$*Me*), −0.26 (m, 2H, *CH*$_2$Me). ^{13}C NMR (75 MHz, 193 K): *δ* 217.8, 211.5 (Me*C*≡*C*Me), 151.0, 150.9, 147.8, 144.9, 143.8, 143.5 (Tp^{Me2}*C*Me), 107.4, 107.2, 106.2 (Tp^{Me2}*C*H), 79.4 (d, $^1J_{CH}$ = 144 ± 5 Hz, Nb*C*HMe), 28.5 (t, $^1J_{CH}$ = 122 ± 5 Hz, *C*H$_2$-Me), 18.3 (q, $^1J_{CH}$ = 123 ± 5 Hz, CH$_2$*Me*), 20.3, 18.0, 15.6, 15.5, 13.8, 13.0, 12.8 (Tp^{Me2}*Me*), 4.1 (q, $^1J_{CH}$ = 123 ± 5 Hz, NbCH*Me*); HMQC correlates protons at *δ* 1.16 and 0.46 with carbons at *δ* 4.1 and 18.3, respectively. **5AR-CS.** Following the general procedure, reaction between Tp^{Me2}NbCl$_2$(MeC≡CMe) (0.840 g, 1.6 mmol) and *sec*-BuMgCl (1.4 mL of a 1.5 M solution, 2.1 mmol) yielded a first crop of crystals from toluene/pentane. The supernatant was collected by filtration and pumped to dryness. The residue was dissolved in a minimum amount of toluene (∼<1 mL), and pentane (∼10 mL) was added to induce crystallization. The supernatant was collected, and the whole procedure was repeated twice. Crystals of diastereomerically pure **5AR-CS** were then collected (0.145 g, 0.27 mmol, 17%). ^{1}H NMR (400 MHz): at 293 K, *δ* 5.94, 5.93, 5.74 (s, 1H each, Tp^{Me2}C*H*), 3.15, 1.82 (s, 3H each, *Me*C≡C*Me*), 2.60, 2.49, 2.35, 2.29, 1.92 (s, 3H each, 1:2:1:1:1, Tp^{Me2}*Me*), 1.65 (m, 1H, *H*CHMe), 0.83 (t, 3H, CH$_2$*Me*), 0.75 (m, 1H, HC*H*Me), 0.65 (m, 1H, *H*CNb); at 193 K, for **5AR-CS*β***, *δ* 5.95, 5.88, 5.76 (s, 1H each, Tp^{Me2}C*H)*, 2.93, 1.73 (s, 3H each, *Me*C≡C*Me*), 2.52, 2.44, 2.39, 2.29, 2.20, 1.79 (s, 3H each, Tp^{Me2}*Me*), 1.47 (br d, 1H, HC*H*Me), 1.30 (br d, 1H, C*H*Me), 1.19 (br d, 3H, CH$_2$*Me*), 0.86 (m, 1H, HC*H*Me), 0.05 (d, 3H, NbCH*Me*); for **5AR-CSα**, *δ* 5.91, 5.81, 5.71 (s, 1H each, Tp^{Me2}C*H*), 3.19, 1.89 (s, 3H each, *Me*C≡C*Me*), 2.53, 2.44, 2.39, 2.35, 2.29 (s, 3H each, Tp^{Me2}*Me*), 1.84 (br d, 3H, CH*Me*), 1.15 (br d, 1H, HC*H*Me), 0.36 (br d, 3H, CH$_2$*Me*), 0.20 (m, 1H, HC*H*Me), −1.14 (br d, 1H, NbC*H*Me). ^{13}C NMR (100 MHz, 193 K): for **5AR-CS*β***, *δ* 217.6, 215.5 (Me*C*≡*C*Me), 150.9, 150.4, 147.7, 144.8, 143.7 (Tp^{Me2}*C*Me), 107.4, 106.9, 106.1 (Tp^{Me2}*C*H), 82.1 (d, $^1J_{CH}$ = 132 Hz, Nb*C*HMe), 19.0 (q, $^1J_{CH}$ = 123 ± 5 Hz, NbCH*Me*), 16.1 (q, $^1J_{CH}$ = 123 ± 5 Hz, CH$_2$*Me*), 14.4 (CH$_2$Me), 21.4, 20.6, 15.6, 15.1, 14.2, 13.0, 13.0 (Tp^{Me2}*Me*); HMQC correlates protons at *δ* 1.19 and 0.05 with carbons at *δ* 16.1 and 19.0, respectively; for **5AR-CSα**: 241.3, 223.9 (MeC≡CMe), 151.1, 151.0, 150.3, 144.6, 144.3, 144.1 (Tp^{Me2}*C*Me), 126.0 (d, $^1J_{CH}$ = 92 Hz, Nb*C*HMe), 32.9 (t br, $^1J_{CH}$ = 130 ± 5 Hz, *C*H$_2$Me), 27.1 (NbCH*Me*), 21.4, 15.2, 14.6, 13.8, 13.2, 12.9, 12.6 (Tp^{Me2}*Me* and CH$_2$*Me*); HMQC correlates proton at *δ* −1.14 with carbon at *δ* 126.0.

Tp^{Me2Cl}NbCl(CH$_2$CH$_2$Me)(PhC≡CMe) (7). Anal. Calcd for $C_{27}H_{34}N_6Cl_4BNb$: C, 47.13; H, 4.98: N, 12.21. Found: C, 47.90; H, 4.71; N, 11.87. ^{1}H NMR (250 MHz, 297 K, benzene-d_6): major rotamer *δ* 6.9−6.85 (m, 5 H, *PhC*≡CMe), 3.60 (m, 1H, HC*H*CH$_2$Me), 3.56 (s, 3H, PhC≡C*Me*), 2.75, 2.06, 1.97, 1.93, 1.87, 1.57 (s, 3H each, Tp^{Me2Cl}*Me*), 1.40 (br m, 1H, CH$_2$*CH*$_2$Me), 0.72 (t, *J* = 7 Hz, 3H, CH$_2$*Me*), 0.60 (br m, 1H, CH$_2$C*H*$_2$Me), 0.40 (m, 1H, *H*CHCH$_2$Me); minor rotamer *δ* 8.10 (d, 2H, *o-Ph*C≡CMe), 7.40 (t, 2H, *m*-PhC≡CMe), 7.25 (t, 1H, *p*-PhC≡CMe), 3.60 (m, 1H, HC*H*CH$_2$Me), 2.82, 2.32, 2.07, 2.03, 1.89, 1.79 (s, 3H each, PhC≡C*Me* and Tp^{Me2}*Me*), 0.58 (s, 3H, CH$_2$CH$_2$*Me*); rotamer ratio, 3.0. ^{13}C NMR (62.9 MHz, 297 K): major rotamer *δ* 250.4, 217.0 (PhC≡*C*Me), 150.3, 149.75, 147.5, 141.6, 141.2, 141.05 (Tp^{Me2}C*Me*), 138.5 (*ipsoC*Ph), 131.9, 129.75, 129.5 (*Ph*), 111.0, 110.6, 110.4 (Tp^{Me2}*C*Cl), 97.8 (dd, $^1J_{CH}$ = 125, 102 Hz, HCHCH$_2$Me), 27.5 (CH$_2$*CH*$_2$Me), 23.2 (PhC≡C*Me)*, 20.0, 13.3, 13.1, 12.3, 11.1, 10.8, 10.6 (Tp^{Me2}Me and CH$_2$CH$_2$*Me*); minor rotamer *δ* 236.4, 228.7 (Ph*C*≡*C*Me), 149.6, 149.2, 146.3, 141.3, 140.9 (Tp^{Me2}C*Me*), 137.8 (*ipsoC*Ph), 129.9, 129.75, 129.3 (*Ph*), 110.8, 110.5, 110.3 (Tp^{Me2}*C*Cl), 100.45 (dd, $^1J_{CH}$ = 130, 108 Hz, HCHCH$_2$Me), 23.0, 19.7, 13.4, 13.3, 12.1, 10.9, 10.5 (Tp^{Me2}Me, CH$_2$CH$_2$*Me* and HCH*C*H$_2$-Me).

Tp^{Me2}NbCl(CH$_2$CH$_2$CH$_2$Me)(MeC≡CMe) (8). Anal. Calcd for $C_{23}H_{37}N_6BClNb$: C, 51.47; H, 6.95: N, 15.67. Found: C, 50.61; H, 6.74; N, 15.12. ^{1}H NMR (300 MHz, benzene-d_6, 300 K): *δ* 5.78, 5.71, 5.57 (s, 1H each, Tp^{Me2}C*H*), 3.40, 2.34 (s, 3H each, *Me*C≡C*Me*), 3.68 (dt, 1H, *J* = 12, 3.4 Hz, HC*H*CH$_2$CH$_2$Me), 2.80, 2.24, 2.15, 2.11, 2.10, 1.83 (s, 3H each, Tp^{Me2}*Me*), 1.60 (m, 1H, CH$_2$C*H*$_2$CH$_2$Me), 1.30 (app sextet, 2H, *J* = 7 Hz, CH$_2$CH$_2$C*H*$_2$Me), 0.83 (t, 3H, *J* = 7 Hz, CH$_2$-CH$_2$CH$_2$*Me*), 0.75 (m, 1H, CH$_2$C*H*$_2$CH$_2$Me), 0.43 (dt, 1H, *J* = 12, 3.4 Hz, 1H, HC*H*CH$_2$CH$_2$Me). ^{13}C NMR (75 MHz, benzene-d_6, 300 K) *δ* 245.7, 224.75 (Me*C*≡*C*Me), 153.0, 152.3, 149.1, 144.1, 144.0, 143.8 (Tp^{Me2}C*Me*), 108.2, 107.7, 107.5 (Tp^{Me2}*C*H), 91.7 (br dd, $^1J_{CH}$ = 125, 110 Hz, HCHCH$_2$Et), 35.7, 28.9 (CH$_2$*CH*$_2$*C*H$_2$Me), 22.8, 21.1 (*Me*C≡C*Me*), 15.6, 15.3, 14.25, 14.2, 13.1, 13.0, 12.6 (Tp^{Me2}*Me* and CH$_2$-CH$_2$CH$_2$*Me*).

Interconvertion of 2α and 2*β* by Spin Saturation Transfer (SST). ^{1}H NMR (400 MHz) SST experiments at different temperatures were obtained according to established procedures.[34−36] In a typical experiment, ∼20 mg of **2** in 0.5 mL of dichloromethane-d_2 (dinitrogen atmosphere, septum-sealed NMR tube) was equilibrated (at least 20 min at each temperature) in the cooled NMR probe below the coalescence temperature of the phenylpropyne methyl singlets of **2α** and **2*β***. At a given temperature (203 K), the T_1 of these protons was first determined by the classical inversion−recovery method. Saturation of the **2*β*** signal (*δ* 3.08) was followed by the observation (90° pulse; 8 scans; acquisition time, 2.720 s; 32 K data points) of the corresponding alkyne signal for **2α** (*δ* 3.60). The intensity decrease of the latter was

monitored against a reference spectrum recorded under identical conditions but with an off resonance (centered at δ 4.12 in this experiment). The rate constant $k_{\beta\rightarrow\alpha}$. for the **2*β*** → **2α** process was obtained from the expression $k_{\beta\rightarrow\alpha}. = (1/T_{12\alpha})[M_{2\alpha}(0)/M_{2\alpha}(\infty) - 1]$ where $M_{2\alpha}(0)$ and $M_{2\alpha}(\infty)$ are the equilibrium magnetizations (signal intensities) of the alkyne methyl signal of **2α**. In a single experiment at 203 K, values of 0.814 s, 5.00 s, 4.25 and 1.08 for $T_{12\alpha}$, saturation time, $M_{2\alpha}(0)$ and $M_{2\alpha}(\infty)$, respectively, gave $k_{\alpha\rightarrow\beta} = 3.61\ s^{-1}$. Experimental data obtained from several experiments are gathered in the Supporting Information.

Thermal Rearrangement of 2 and 2-*d*$_6$. The kinetic data at 323 K were obtained by monitoring (^{1}H NMR, 250 MHz, toluene-d_8) the disappearance of the alkyne methyl signal at δ 3.8. The disappearance of **2** (or **2**-d_6) was quantified by integration against the whole $Tp^{Me2}CH$ resonances between δ ~6.1 and 5.1; ~15 mg of **2** (or **2**-d_6) was dissolved under dinitrogen in toluene-d_8 (0.5 mL, [**2**] $\approx 4 \times 10^{-2}$ M) in a 5-mm NMR tube that was sealed with a septum and ParaFilm. The tube was introduced into the preheated probe of the NMR spectrometer. After 15 min of thermal equilibration, an automatic acquisition program was used to collect the spectra every 30 min (32 scans; acquisition time, 3.064 s; 16 K data points; repetition delay, 2.0 s). The reaction was monitored for approximately three half-lives, but the kinetics were well-behaved for approximately two half-lives. The results of a typical first-order treatment are provided in the Supporting Information.

Crystallographic Studies. Single crystals of **2**, **5AR-CS** and **5CR-AS** were obtained from toluene/pentane or hexane solutions. A summary of experimental and refinement data is presented in the Supporting Information. The data collection ($T = 160$ K) was performed on an STOE IPDS diffractometer using graphite monochromatized MoKα radiation. The structures were solved by direct methods using SIR92[60] and subsequent difference Fourier maps. Absorption corrections were applied for **5CR-AS**. The refinement was carried out using the CRYSTALS package.[61] All atoms except hydrogens were anisotropically refined. Several hydrogen atoms were observed in difference Fourier maps. For the three structures, only B−H, α-, and *β*-hydrogens, where appropriate, were considered and subsequently refined using an isotropic equivalent thermal parameter. For **5AR-CS**, only the nonagostic methylene hydrogen of the *sec*-butyl group was located. Other hydrogen atoms were included in the calculations in idealized positions (C−H = 0.96 Å) using an isotropic thermal parameter 1.2× that of the carbon atom to which they were attached. Full matrix least-squares refinements were carried out by minimizing the function $\sum w(|F_o| - |F_c|)^2$, where F_o and F_c are the observed and calculated structure factors. Weighting schemes were subsequently introduced, with $w = w'[1 - (\Delta F/6\sigma(F))^2]^2$.[62] Models reached convergence with $R = \sum(|F_o| - |F_c|)/\sum|F_o|$, $R_w = [\sum w(|F_o| - |F_c|)^2/\sum w(|F_o|)^2]^{1/2}$ being 0.0289 and 0.0281 (2412 reflections with $I > 2\sigma(I)$, 342 parameters) for **2**; 0.0280 and 0.0288 (3750 reflections with $I > \sigma(I)$, 309 parameters) for **5CR-AS**; and 0.0513 and 0.0429 (3486 reflections with $I > 3\sigma(I)$, 307 parameters) for **5AR-CS**. Plots of molecular structures were performed by using the software CAMERON.[63]

Computational Details. Calculations were performed using the hybrid quantum mechanics/molecular mechanics (QM/MM) method IMOMM.[37] The program used was built from modified versions of two standard programs, Gaussian92/dft[64] and mm3(92).[65] The QM region was defined by $[Nb(NH{=}CH_2)_3(Cl)(CH(CH_3)_2)(HC{\equiv}CH)]^+$. The most arguable aspect of this QM/MM partition, the modeling of the electronic effects of the Tp^{Me2} ligand by $(NH{=}CH_2)_3^+$, has been shown to produce satisfactory results in previous studies.[23,66] The QM part of the calculations used the Becke3LYP density functional. A pseudopotential was used for the internal electrons of niobium,[67] and a valence double-ζ basis set was used for all atoms,[67−70] with the addition of a polarization d shell on Cl.[70] The MM part of the calculations on the full system used the mm3(92) force field.[71] van der Waals parameters for the niobium atom were taken from the UFF force field,[72] and torsional contributions involving dihedral angles with the metal atom in a terminal position were set to zero.

Parameters missing in the standard mm3(92) force field, such as several of those involving boron, were taken from the force field implementation in the Chem3D package[73] or were estimated from the values for similar atoms. The mm3(92) default value for the van der Waals radius of chlorine was replaced by a more appropiate value for inorganic species.[74] All geometrical parameters were optimized except the bond distances involved in the QM/MM interface. The frozen QM values were 1.10 Å for C−H and 1.00 Å for N−H; the frozen MM values were 1.5247 Å for C(ring)−C(alkyl), 1.387 Å for C(ring)−C(ring), and 1.378 Å for N−N.

Acknowledgment. Bruno Donnadieu (acquisition of X-ray data), Dr Yannick Coppel and Francis Lacassin (high field NMR) are thanked for their skilfull assistance. J.E.M. acknowledges the support of the E.U. in the form of a Marie Curie Fellowship.

Note Added in Proof: During the time this article was being printed, a related equilibrium between α- and *β*-agostic rotamers in a $TaCH_2CH_3$ group has been described.[75]

Supporting Information Available: Tables providing full structural details and fractional atomic coordinates, anisotropic thermal parameters, and bond lengths and angles for compounds **2**, **5CR-AS** and **5AR-CS**. Tables of T_1 and rate constants $k_{\alpha\rightarrow\beta}$ for **2** and **5AR-CS** as a function of temperature as determined by SST experiments, and accompanying plots of ln*k* and ln(k/T) vs 1/*T*. Plots of ln *K* vs 1/*T* for **2** and **2**-d_6. A first-order kinetic plot for the rearrangement of **2**. This material is available free of charge via the Internet at http://pubs.acs.org.

JA0038169

(60) Altomare, A.; Cascarano, G.; Giacovazzo, G.; Guargliardi, A.; Burla, M. C.; Polidori, G.; Camalli, M. *J. Appl. Crystallogr.* **1994**, *27*, 435.
(61) Watkin, D. J.; Prout, C. K.; Carruthers, R. J.; Betteridge, P. *CRYSTALS Issue 10*; University of Oxford: Oxford, 1996.
(62) Carruthers, J. R.; Watkin, D. J. *Acta Crystallogr.* **1979**, *A35*, 698.
(63) Watkin, D. J.; Prout, C. K.: Pearce, L. J. *CAMERON*; University of Oxford: Oxford, 1996.
(64) Frisch, M. J.; Trucks, G. W.; Schlegel, H. B.; Gill, P. M. W.; Johnson, B. G.; Wong, M. W.; Foresman, J. B.; Robb, M. A.; Head-Gordon, M.; Replogle, E. S.; Gomperts, R.; Andres, J. L.: Raghavachari,-K.; Binkley, J. S.; Gonzalez, C.; Martin, R. L.; Fox, D. J.; Defrees, D. J. B *Gaussian 92/DFT*; Gaussian, Inc: Pittsburgh, PA, 1993.
(65) Allinger, N. L. *mm3(92)*; QCPE: Bloomington, IN, 1992.
(66) Cucurull-Sánchez, L.; Maseras, F.; Lledós, A. *Inorg. Chem. Commun.* **2000**, *3*, 589−592.
(67) Hay, P. J.; Wadt, W. R. *J. Chem. Phys.* **1985**, *82*, 299−310.
(68) Wadt, W. R.; Hay, P. J.*J. Chem. Phys.* **1985**, *82*, 284−298.
(69) Hehre, W. J.; Ditchfield, R.; Pople, J. A. *J. Chem. Phys.* **1972**, *56*, 2257−2261.
(70) Francl, M. M.; Pietro, W. J.; Hehre, W. J.; Binkley, J. S.; Gordon, M. S.; DeFrees, D. J.; Pople, J. A. *J. Chem. Phys.* **1982**, *77*, 3654−3665.
(71) Allinger, N. L.; Yuh, Y. H.; Lii, J. H. *J. Am. Chem. Soc.* **1989**, *111*, 8551−8565.
(72) Rappé, A. K.; Casewit, C. J.; Colwell, K. S.; Goddard, W. A., III; Skiff, W. M. *J. Am. Chem. Soc.* **1992**, *114*, 10024−10035.
(73) *Chem3D*; CambridgeSoft Corporation: Cambridge, MA 02139.
(74) Ujaque, G.; Maseras, F.; Eisenstein, O. *Theor. Chem. Acc.* **1997**, *96*, 146−150.
(75) Fryzuk, M. D.; Johnson, S. A.; Rettig, S. J. *J. Am. Chem. Soc.* **2001**, *123*, 1602−1612.